

1 **Effects of dust aerosols on tropospheric chemistry during a typical pre-**
2 **monsoon season dust storm in northern India**

3 Rajesh Kumar^{1, 2}, M. C. Barth², S. Madronich², M. Naja³, G. R. Carmichael⁴, G. G. Pfister², C.
4 Knote², G. P. Brasseur^{1, 5}, N. Ojha³ and T. Sarangi³

5 ¹Advanced Study Program, National Center for Atmospheric Research, Boulder, USA

6 ²Atmospheric Chemistry Division, National Center for Atmospheric Research, Boulder, USA

7 ³Aryabhata Research Institute of Observational Sciences, Nainital, India

8 ⁴Center for Global and Regional Environmental Research, University of Iowa, Iowa City, IA

9 52242, USA

10 ⁵Climate Service Center, Helmholtz Zentrum Geesthacht, Hamburg, Germany

11

12 Correspondence to: Rajesh Kumar (rkumar@ucar.edu)

13

14 Running title: Dust aerosols and tropospheric chemistry

15

16

1 **Abstract**

2 This study examines the effect of a typical pre-monsoon season dust storm on tropospheric
3 chemistry through a case study in northern India. Dust can alter photolysis rates by scattering and
4 absorbing solar radiation, and provide surface area for heterogeneous reactions. We use the
5 Weather Research and Forecasting model coupled with Chemistry (WRF-Chem) to simulate the
6 dust storm that occurred during 17-22 April 2010 and investigate the contribution of different
7 processes on mixing ratios of several key trace gases including ozone, nitrogen oxides, hydrogen
8 oxides, methanol, acetic acid and formaldehyde. We revised the Fast Troposphere Ultraviolet
9 Visible (F-TUV) photolysis scheme to include effects of dust aerosols on photolysis rates in a
10 manner consistent with the calculations of aerosol optical properties for feedback to the
11 meteorology radiation schemes. In addition, we added twelve heterogeneous reactions on the
12 dust surface, for which six reactions have relative humidity dependent reactive uptake
13 coefficients (γ). The inclusion of these processes in WRF-Chem is found to reduce the difference
14 between observed and modeled O_3 from 16 ± 9 to 2 ± 8 ppbv and that in NO_y from 2129 ± 1425 to
15 372 ± 1225 pptv compared to measurements at the high altitude site Nainital in the central
16 Himalayas, and reduce biases by up to 30% in tropospheric column NO_2 compared to OMI
17 retrievals. The simulated dust storm acted as a sink for all the trace gases examined here and
18 significantly perturbed their spatial and vertical distributions. The reductions in these gases are
19 estimated as 5-100% and more than 80% of this reduction was due to heterogeneous chemistry.
20 The RH dependence of γ is also found to have substantial impact on the distribution of trace
21 gases, with changes of up to 20-25% in O_3 and HO_2 , 50% in H_2O_2 and 100% in HNO_3 . A set of
22 sensitivity analyses revealed that dust aging could change H_2O_2 and CH_3COOH levels by up to
23 50% but has a relatively small impact on other gases.

1 **1. Introduction**

2 Dust aerosols have gained considerable attention in the recent years not only because they
3 constitute a major fraction of the particulate matter in the troposphere but also because they have
4 important implications for air quality, visibility, the Earth's radiation budget (e.g. Haywood and
5 Boucher, 2000; Seinfeld et al., 2004), biogeochemistry (e.g. Jickells et al., 2005), hydrological
6 cycles (e.g. Miller et al., 2004, Zhao et al., 2011), and atmospheric chemistry (e.g. Dentener et
7 al., 1996; Wang et al., 2012). The significance of dust aerosols for atmospheric chemistry has
8 been manifested through several experimental (e.g. Goodman et al., 2000; Underwood et al.,
9 2001, Li et al., 2006; Preszler Prince et al., 2007, Wagner et al., 2008; Cwiertny et al., 2008;
10 Pradhan et al., 2010, Crowley et al., 2010; Chen et al., 2011; Bedjanian et al., 2013a, 2013b) and
11 modeling studies (e.g. Zhang et al., 1994; Dentener et al., 1996; Zhang and Carmichael, 1999;
12 Tang et al., 2004; Martin et al., 2003; Bauer et al., 2004; Tie et al., 2005; Hodzic et al., 2006;
13 Zhu et al., 2010; Wang et al., 2012) during the past two decades.

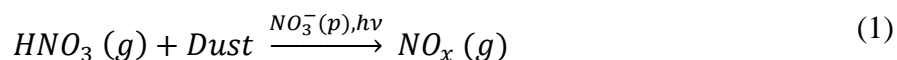
14
15 Dust aerosols can influence atmospheric chemistry by affecting the photolysis rate coefficients
16 through interaction with incoming solar radiation and by providing surface area for
17 heterogeneous chemistry and deposition of different trace gases. It has been suggested that
18 mineral dust aerosols are responsible for 5-20% reduction in photolysis rate coefficients of ozone
19 (O_3) and nitrogen dioxide (NO_2) throughout the Northern Hemisphere (e.g. Martin et al., 2003;
20 Tie et al., 2005; Ying et al., 2011). These changes in photolysis rate coefficients then decrease
21 the annual mean global concentration of hydroxyl radical (OH) by 9%, which in turn leads to
22 increases in the concentrations of several volatile organic compounds (Martin et al., 2003).
23 Heterogeneous reactions on dust surfaces generally reduce the concentration of key atmospheric

1 trace gases such as O₃, nitrogen oxides, sulfur oxides and hydrogen oxides, but the amount of
2 reported reduction in these gases varies widely, indicating that heterogeneous chemistry on dust
3 surfaces is still not well understood. For example, the decreases in surface O₃ are reported as 5-
4 40% by different studies (Zhang et al., 1994; Dentener et al., 1996; Zhang and Carmichael, 1999;
5 Tang et al., 2004; Bauer et al., 2004; Zhu et al., 2010, Wang et al., 2012). Likewise, the
6 decreases for sulfur dioxide (SO₂), nitrogen oxides and hydrogen oxides are reported as 10-50%,
7 16-100% and 11-59% respectively.

8
9 Even though this study is focused on the impact of heterogeneous processes on dust surfaces on
10 the tropospheric chemistry in northern India, it is worth mentioning other implications of
11 heterogeneous chemistry here. The heterogeneous uptake of trace gases can potentially affect the
12 physiochemical properties of dust aerosols and enhance their ability to act as cloud condensation
13 nuclei (CCN). Dust particles are generally hydrophobic when they are emitted but become
14 hygroscopic as they travel in the atmosphere and become coated with nitrate, sulfate and
15 organics (e.g. Levin et al., 1996; Kelly et al., 2007; Hatch et al., 2008). The coating process will
16 also modify the distributions of dust as well as sulfate and nitrate aerosols, which in turn will
17 increase the scattering of solar radiation by aerosols. The increase in size of dust particles due to
18 coating will increase the probability of their removal from the atmosphere and such coated
19 particles will experience less long-range transport.

20
21 Box and regional modeling studies have focused mostly on heterogeneous chemistry on East
22 Asian and Saharan dust aerosols, whereas there have been no such studies over the northern
23 Indian region where dust storms occur frequently during the pre-monsoon (March, April, May;

1 MAM) season (e.g. Prasad and Singh, 2007; Hegde et al., 2007). Global modeling studies have
2 suggested that heterogeneous chemistry on dust aerosols can reduce surface O₃ in northern India
3 by 4-10% (e.g. Dentener et al., 1996; Bauer et al., 2004). However, there has been a considerable
4 improvement in our understanding of heterogeneous chemistry on dust aerosols since these
5 global modeling studies were conducted. A major advancement has been the demonstration of
6 relative humidity (RH) dependence of the reactive uptake coefficient for several species such as
7 O₃ (Cwiertny et al., 2008), HNO₃ (Liu et al., 2008), OH (Bedjanian et al., 2013a), HO₂
8 (Bedjanian et al., 2013b), SO₂ (Preszler Prince et al., 2007) and H₂O₂ (Pradhan et al., 2010). The
9 renoxification process (Equation 1), which was ignored in those global modeling studies, is also
10 included here. In this process, the uptake of gas-phase HNO₃ by dust particles is followed by
11 release of gas-phase NO_x (both NO and NO₂) in the presence of broadband radiation (e.g. Chen
12 et al., 2011).



13 where (g) and (p) represent the species in gas and particle phase respectively. Therefore, it is
14 essential to reassess the importance of dust aerosols for tropospheric chemistry in northern India
15 by taking into account these recent advancements.

16
17 In light of the above conditions, this manuscript examines the effects of dust aerosols on the
18 distribution of many key trace gases including O₃, nitrogen oxides, hydrogen oxides, methanol,
19 acetic acid and formaldehyde by incorporating the updated information on heterogeneous
20 reactive uptake of trace gases in MOZCART chemical mechanism of Weather Research and
21 Forecasting model coupled with Chemistry (WRF-Chem). We also revise the Fast Troposphere
22 Ultraviolet Visible (F-TUV) scheme to include effects of dust aerosols on photolysis rates. This

1 extended configuration of WRF-Chem is then used to simulate the impact of a typical pre-
2 monsoon season dust storm on the regional tropospheric chemistry in northern India. This dust
3 storm occurred during 17-22 April 2010 in northern India. A detailed analysis of the evolution of
4 this dust storm, dust emissions and their effect on local to regional scale aerosol optical
5 properties and radiation budget are presented in a companion paper (Kumar et al., 2014).

6
7 We begin by describing the WRF-Chem configuration and implementation of effect of dust
8 aerosols on photolysis rates and heterogeneous chemistry on dust surfaces. We next briefly
9 describe the observations used to evaluate the WRF-Chem trace gas results. In the Results
10 section, we show the importance of dust effects on tropospheric gas chemistry by comparing the
11 model results with observations. Sensitivity simulations are used to discuss the contributions of
12 different processes and evaluate the uncertainties in the representation of heterogeneous
13 chemistry. We conclude that heterogeneous chemistry mostly, partly dust-modified photolysis
14 rates, improve the agreement between model results and observations, and that these processes
15 lead to a reduction in O_3 , H_2O_2 , and HNO_3 .

16 17 **2. The WRF-Chem Model**

18 The Weather Research and Forecasting Model version 3.4.1 (Skamarock et al., 2008) coupled
19 with Chemistry (Grell et al., 2005; Fast et al., 2006) is used here to simulate the distribution of
20 trace species. The simulation domain has 120 x 90 x 51 grid points in (x, y, z) direction with a
21 grid spacing of 30 x 30 km² extending in the vertical up to 10 hPa. The static geographical fields,
22 such as terrain height, vegetation fraction, soil properties and land-use etc., are interpolated from
23 10 min (~ 19 km) United States Geological Survey (USGS) data to the model domain by using

1 the WRF preprocessing system (WPS). The initial and lateral boundary conditions for the
2 meteorological fields are obtained from the National Center for Environmental Predictions
3 (NCEP) Final Analysis (FNL) fields available every 6h at a spatial resolution of $1^{\circ} \times 1^{\circ}$. The
4 resolved scale cloud physics is represented by the Thompson microphysics scheme (Thompson
5 et al., 2004) and sub-grid scale effects of convective and shallow clouds are parameterized
6 according to the Kain-Fritsch convective scheme (Kain, 2004). The short- and long-wave
7 radiative processes in the atmosphere are represented by the Rapid Radiative Transfer Model
8 (RRTM) (Mlawer et al., 1997). For surface processes, the model setup uses the NOAH Land
9 Surface model (Chen and Dudhia, 2001) and MM5 similarity scheme (Beljaars, 1994). The
10 vertical sub-grid scale fluxes due to eddy transport in the planetary boundary layer (PBL) and the
11 free troposphere are parameterized according to the Yonsei University (YSU) boundary layer
12 scheme (Hong et al, 2006). Four dimensional data assimilation (FDDA) is applied to limit model
13 errors in the simulated meteorological fields (Lo et al., 2008).

14
15 Gas-phase chemistry is represented by the Model for Ozone and Related chemical Tracers,
16 version 4 (MOZART-4, Emmons et al., 2010), and aerosol processes by the GOCART bulk
17 aerosol scheme (Chin et al., 2002; Pfister et al., 2011). The GOCART model simulates five
18 major tropospheric aerosol types including sulfate, organic carbon, black carbon, dust and sea-
19 salt, assuming externally mixed aerosols. The GOCART model does not have an aerosol
20 thermodynamics module. The emissions of sea-salt (four size bins) and dust aerosols (five size
21 bins) are calculated online within the model. The dust emission scheme is based on Ginoux et al.
22 (2001) and calculates size resolved dust emissions online in five size bins ranging from 0.73-8.0
23 μm (effective radius) using the following equation:

$$F_p = \begin{cases} CSs_p u_{10m}^2 (u_{10m} - u_t) & \text{if } u_{10m} > u_t \\ 0 & \text{otherwise} \end{cases} \quad (2)$$

1 where F_p ($\text{kg m}^{-2} \text{s}^{-1}$) represents the emission flux for size bin p , C is an empirical proportionality
2 constant ($\text{kg m}^{-5} \text{s}^2$), S is the source function representing the fraction of alluvium available for
3 wind erosion, s_p is the fraction of each size class of dust in the emission, u_{10m} (m s^{-1}) is the
4 horizontal wind speed at 10 m above the surface and u_t is the threshold velocity (m s^{-1}) below
5 which dust emission does not occur and is a function of particle size and density, air density and
6 surface moisture. In principle, S should be based on observations of alluvium in the model
7 domain but such observations do not exist. Therefore, S is obtained by comparing elevation of
8 each grid cell with its surrounding hydrological basin spread over an area of $10^0 \times 10^0$. Thus, S
9 does not provide the exact amount of alluvium present but it provides information about the most
10 probable locations of sediments. The map of S is then compared with vegetation map derived
11 from Advanced Very High Resolution Radiometer (AVHRR) data (DeFries and Townshend,
12 1994) and only the bare soil surfaces are considered as possible dust sources. In WRF-Chem, the
13 source function is provided as an input static geographical field through the WRF preprocessing
14 system (WPS). The threshold wind velocity u_t is estimated as:

$$u_t = \begin{cases} A \sqrt{\frac{(\rho_p - \rho_a)g\Phi_p}{\rho_a}} & (1.2 + 0.2 \log_{10} w), \quad \text{if } w < 0.5 \\ \infty & \text{otherwise} \end{cases} \quad (2a)$$

15 where $A = 6.5$ is a dimensionless parameter, w is the surface wetness (0.001-1), Φ_p is the particle
16 diameter, g is the acceleration of gravity, ρ_a and ρ_p are the air and particle density respectively.
17 More information about estimation of S and u_t can be obtained from Ginoux et al. (2001).

18

1 The tuning factor C does not have any physical meaning. Its default value was proposed initially
2 as $1 \times 10^{-9} \text{ kg m}^{-5} \text{ s}^2$ (Ginoux et al., 2001) but we have set it to $2.2 \times 10^{-8} \text{ kg m}^{-5} \text{ s}^2$ as the latter value
3 led to a good agreement between model and Aerosol Robotic Network (AERONET) measured
4 aerosol optical depth and Angström exponent at seven sites in the model domain (Kumar et al.,
5 2014). A factor of magnitude difference in the value of C results partly from the use of analysis
6 nudging (FDDA) in this study as nudging leads to lower wind speeds. A sensitivity experiment
7 showed that similar dust emissions could be obtained with a C value of $9 \times 10^{-9} \text{ kg m}^{-5} \text{ s}^2$ without
8 applying analysis nudging. However, we chose to use analysis nudging as the model
9 configuration with analysis nudging is found to better reproduce the variations in observed
10 aerosol optical properties as compared to one without analysis nudging (not shown).

11
12 Anthropogenic emissions of CO , NO_x , SO_2 , NH_3 , OC and BC and non-methane volatile organic
13 compounds (NMVOC) are taken from the MACCity emission inventory (Granier et al., 2011)
14 and emissions for $\text{PM}_{2.5}$ and PM_{10} are taken from the Intercontinental Chemical Transport
15 Experiment – Phase B (INTEX-B) inventory (Zhang et al., 2009). Daily varying emissions of
16 trace species from biomass burning are taken from the Fire Inventory from NCAR version 1
17 (FINN v1) (Wiedinmyer et al., 2011) and distributed vertically in the model following the online
18 plume-rise module (Freitas et al., 2007). Note that FINN v1 accounts only for open biomass
19 burning and the residential biomass burning is included in anthropogenic emissions. Biogenic
20 emissions of trace species from terrestrial ecosystems are calculated online using the Model of
21 Emissions of Gases and Aerosols from Nature (MEGAN) version 2.04 (Guenther et al., 2006).
22 The aerosols are allowed to provide feedback to the radiation scheme in the simulations but
23 through direct effects only. The simulations start on 10 April 2010 at 0000 GMT and end on 25

1 April 2010 at 1800 GMT. The first three days of the model output are removed from the analysis
2 to allow the model to spin up.

3

4 **2.1 Effect of aerosols on photolysis rates in WRF-Chem**

5 In this study, we use the Fast-Troposphere Ultraviolet Visible (F-TUV) scheme to calculate
6 photolysis rates for the MOZCART chemical mechanism. The F-TUV scheme is a simplified
7 version of the National Center for Atmospheric Research's (NCAR) TUV model (Madronich and
8 Weller, 1990) and is designed to reduce the computational costs associated with TUV (Tie et al.,
9 2005). The F-TUV model utilizes the same physical processes as the TUV model except that the
10 number of wavelengths in the TUV spectra (121-750 nm) was reduced from 140 to 17, making it
11 eight times faster than the TUV model. The differences in the calculated photolysis rate
12 coefficients between the TUV and F-TUV model are reported to be less than 5% (Tie et al.,
13 2005).

14

15 To include the effect of aerosols on photolysis rates, the F-TUV photolysis scheme in WRF-
16 Chem calculates optical properties (optical depth, single scattering albedo and asymmetry
17 parameter) for black carbon, organic carbon, sulphate and sea-salt aerosols, and passes them to a
18 two-stream radiative transfer module where they interact with radiation to affect photolysis rate
19 coefficients. These optical properties are also calculated in the aerosol optical driver of WRF-
20 Chem and are used for feedback of aerosols on the meteorology radiation schemes. Here, we
21 make use of the optical driver calculated aerosol optical properties in F-TUV photolysis scheme
22 to be consistent between the effects of aerosols on radiation and photolysis rate coefficients. This
23 coupling automatically accounts for the effect of dust aerosols on photolysis rates in WRF-

1 Chem, which was missing in the original F-TUV scheme. Further details regarding the coupling
2 of the optical driver to the F-TUV photolysis scheme can be found in the supplementary
3 material.

4

5 **2.2 Heterogeneous chemistry on dust surface in WRF-Chem**

6 This study also extends the ability of the MOZCART chemical mechanism of WRF-Chem to
7 simulate heterogeneous chemistry on the surface of dust particles by including 12 heterogeneous
8 reactions listed in Table 1. The uptake of these gases on dust particles is assumed to be
9 irreversible (Zhang and Carmichael, 1999) and does not add to the aerosol mass in the model
10 because the GOCART model does not have a thermodynamics module. However, recent
11 laboratory experiments have shown that the uptake of HNO_3 (Chen et al., 2011) is associated
12 with release of gas phase NO_x , and uptake of OH (Bedjanian et al., 2013a) and HO_2 (Bedjanian
13 et al., 2013b) are associated with the release of gas-phase H_2O_2 . The production of these gas
14 phase species from heterogeneous chemistry is taken into account in this study. The production
15 of NO_x from HNO_3 uptake is observed only in the presence of broadband irradiation with a yield
16 of about 50% (Chen et al., 2011), and thus the reaction of HNO_3 is set to yield 0.5 NO_2 during
17 daytime in this study. This yield of 0.5 results from the assumption that all HNO_3 molecules
18 reacting with dust particles adsorb to the surface but HNO_3 has been observed to be lost
19 irreversibly when reacting with CaCO_3 and adsorb to the surface when reacting with other
20 minerals (e.g. Al_2O_3 , Fe_2O_3 , and TiO_2) (Grassian, 2002). For Indian dust particles, the abundance
21 of CaCO_3 is estimated to be about 20% (Peterson, 1968). If we assume that HNO_3 will react with
22 the remaining 80% of the minerals adsorbing to the surface, the yield should be 0.4. However,
23 our assumption of a yield of 0.5 should not affect the model results significantly here as it is

1 shown later (section 4.3) that the renoxification process leads only to a small change in NO_x
 2 values. The yields for H₂O₂ from reactions of OH and HO₂ with dust particles are reported to be
 3 5% (Bedjanian et al., 2013a) and 10% (Bedjanian et al., 2013b) respectively and are set
 4 accordingly. These numbers differ from previous studies, which have assumed a 100%
 5 conversion of HO₂ and 0% conversion of OH into H₂O₂ (e.g. Zhu et al., 2010; Wang et al.,
 6 2012).

7
 8 The pseudo first order reaction rate coefficient (s⁻¹) for the loss of a gas phase species g due to
 9 heterogeneous uptake by dust particles is calculated following Heikes and Thompson (1983) as:

$$k_g = \sum_{i=1}^5 \frac{4\pi r_i D_g V N_i}{1 + K_n [\chi + 4(1 - \gamma)/3\gamma]} \quad (3)$$

10 where i = 1, 5 represents five dust size bins used by the GOCART model, r_i and N_i represents the
 11 effective radius (cm) and number density (particles cm⁻³) of particles in size bin i, V is the
 12 ventilation coefficient and taken as unity, D_g represents the gas-phase molecular diffusion
 13 coefficient of gas molecule g (cm² s⁻¹) and is calculated following Jacobson (2005) as:

$$D_g = \frac{5}{16\rho_a A d_g^2} \sqrt{\left(\frac{m_a + m_g}{m_g}\right) \frac{RT m_a}{2\pi}} \quad (4)$$

14 where ρ_a is atmospheric mass density (g cm⁻³), A is the Avogadro's number (6.022 x 10²³
 15 molecules mol⁻¹), d_g is the collision diameter (cm) of gas molecule g, R is the universal gas
 16 constant (8.31451 x 10⁷ g cm² s⁻² mol⁻¹ K⁻¹), T is the absolute temperature (K), m_a (g mol⁻¹) and
 17 m_g (g mol⁻¹) are the molecular weights of air and gas respectively. In equation (3), K_n is the
 18 dimensionless Knudsen number defined as the ratio of the effective mean free path of a gas
 19 molecule in air (λ) to the effective particle radius r_i. χ represents a correction factor for
 20 anisotropic movement and is calculated as follows:

$$\chi = \frac{\left(\frac{4}{3} K_n + 0.71\right)}{K_n + 1} \quad (5)$$

1 WRF-Chem model simulates the mass mixing ratio (M_i in g g^{-1}) of dust particles, and the use of
2 equation (3) requires the conversion of mass mixing ratios to the number concentration. This is
3 performed using the following equation:

$$N_i = \frac{M_i \rho_a}{\left(\frac{4}{3} \pi r_i^3\right) \rho_p} \quad (6)$$

4 where ρ_p (g cm^{-3}) represents the mass density of the dust particles and are taken as 2.5 and 2.65 g
5 cm^{-3} to represent clay and silt in GOCART (Ginoux et al., 2001).

6
7 The reaction uptake coefficient (γ) is the most important parameter in the calculation of k_g , but
8 the uncertainties in γ are very large and have been reported as more than three orders of
9 magnitudes for certain species such as O_3 and HNO_3 (Goodman et al., 2000; Underwood et al.,
10 2001; Michel et al., 2002). Such large uncertainties make the choice of γ very difficult. Since this
11 study is focusing on Thar Desert dust aerosols for which information on heterogeneous
12 chemistry kinetics is not available we use the best guess values reported for East Asian dust
13 aerosols (Zhu et al., 2010) for the γ values of dry dust particles except for OH and HO_2 . The γ
14 values for OH and HO_2 are taken from Bedjanian et al. (2013a, b). The applied γ values for dry
15 dust particles are shown in Table 1 and vary from 2.1×10^{-6} for NO_2 to 0.18 for OH. Lower and
16 upper bounds of γ reported in the literature are also shown in Table 1. Further information about
17 available measurements of γ for different species can be found in Zhu et al. (2010).

18

19 Many laboratory studies have also demonstrated the dependence of γ on relative humidity (RH),
20 but such a RH dependence has generally been ignored in previous modeling studies (e.g.

1 Dentener et al., 1996; Zhu et al., 2010; Wang et al., 2012). In this study, we include the RH
2 dependence of γ for O₃ (Cwiertny et al., 2008), HNO₃ (Liu et al., 2008), OH (Bedjanian et al.,
3 2013a), HO₂ (Bedjanian et al., 2013b), H₂O₂ (Pradhan et al., 2010), and SO₂ (Preszler Prince et
4 al., 2007). The variations of γ with relative humidity for different trace gases are shown in Figure
5 1. The value of γ increases with RH for HNO₃, SO₂ and H₂O₂ while it decreases with RH for O₃,
6 OH and HO₂. The rate coefficients, i.e., k_g values, are estimated to be of the order of 10^{-3} - 10^{-5} s⁻¹
7 for OH, HO₂, H₂O₂, HNO₃, NO₃, N₂O₅ and CH₃COOH, and of the order of 10^{-7} - 10^{-8} s⁻¹ for O₃,
8 NO₂, SO₂, CH₃OH and CH₂O.

9
10 The aging of dust particles through heterogeneous uptake of acidic gases and organic compounds
11 is another important process that can influence the uptake of trace gases by dust particles.
12 However, the dependence of k_g on aging of mineral dust aerosols is complex and not well
13 understood. For example, the reactive uptake of O₃ (Usher et al., 2003) on HNO₃ and SO₂
14 processed dust particles is reported to increase or decrease depending on the mineralogy of the
15 particle, coverage of the coatings, as well as ambient RH. Due to the complexity of processes
16 involved and lack of information on all 12 heterogeneous reactions, the effect of atmospheric
17 processing of dust particles is not included in this study except for a set of sensitivity simulations
18 conducted to highlight the importance of this aging process. The treatment of dust aging for
19 those sensitivity simulations is presented below.

20

21 **2.3 Atmospheric aging/processing of dust particles**

22 Laboratory experiments have shown that reactive uptake of O₃ decreases by about 70% on dust
23 particles processed with HNO₃ (leading to nitrate coating) while it increases by about 33% on

1 dust particles processed with SO₂ as O₃ reacts with surface bound sulfites/bisulfites to form
2 sulfate (Usher et al., 2003). We have made an attempt here to simulate these changes in dust
3 reactivity and quantify their impact on surface O₃. The simulation of these changes requires
4 partitioning of fresh and aged dust particles and is done using the following procedure: in
5 addition to total dust, two artificial dust tracers called “fresh_dust” and “aged_dust” are
6 introduced into the model to keep track of fresh and aged dust particles. These tracers are
7 included for all five size bins and thus we have a total of 10 tracers in the model. All these
8 tracers undergo the same transport and deposition processes as the original dust tracers.

9
10 The emissions of fresh dust particles are set equal to the emissions of total dust while the
11 emissions of aged dust particles are set to zero. The initial and boundary conditions for fresh dust
12 particles are set equal to those for total dust while those for aged dust particles are set to zero
13 because the MOZART-4 output used for providing initial and boundary conditions does not
14 include such a classification. The assumption that all dust particles entering into the model
15 domain are fresh may introduce some uncertainty in the model results. However, such an
16 uncertainty is anticipated to have a small contribution in the case presented here, as two model
17 runs with and without including the regional dust emissions showed that most of the dust loading
18 over the model domain came from emissions within the model domain during 17-22 April 2010.

19
20 The number concentration (particles cm⁻³) of aged ($N_{a,i}$, $i=1, 5$ represent five size bins) and fresh
21 ($N_{f,i}$) dust particles is updated every time step as follows for each gas g considered: first, the
22 number of molecules of gas g needed to completely coat one dust particle of a given size with a
23 monolayer ($n_{ml,g,i}$) is calculated as the ratio of surface area of the dust particle to the surface area

1 occupied by a gas molecule. Second, the total number of gas molecules of g that can potentially
2 adsorb to dust particles ($n_{\text{pot},g,i}$) is calculated by multiplying k_g (s^{-1}) estimated in equation (3) with
3 gas concentration (molecules cm^{-3}) and time step (180 s in this case). The ratio $n_{\text{pot},g,i}/n_{\text{ml},g,i}$ then
4 provides the number concentration increment $\Delta N_{a,g,i}$ of dust particles that could have aged (i. e.
5 been completely coated with a monolayer of gas) during this time step. The sum of the
6 increments $\Delta N_{a,g,i}$ due to all gases considered in coating gives the total increment in aged
7 particles $\Delta N_{a,i}$. $\Delta N_{a,i}$ is then subtracted from the number concentration of fresh dust particles $N_{f,i}$
8 and added accordingly to the number concentration of aged particles $N_{a,i}$.

9
10 The reactions of HNO_3 , NO_2 , NO_3 and N_2O_5 with dust particles are assumed to coat dust
11 particles with nitrate and that of SO_2 is assumed to coat them with sulfate. All gases are given
12 equal probability to react with dust particles, and in case the number concentration of fresh dust
13 particles is limiting, then $\Delta N_{a,i} > N_{f,i}$, which would lead to negative number concentrations of
14 $N_{f,i}$. To overcome this problem, $N_{a,i}$ and $N_{f,i}$ are set to $N_{f,i}$ and zero respectively. This approach
15 leads to mass conservation of tracers, and the sum of fresh and aged dust particle concentrations
16 is always equal to the total dust number concentration. Both fresh and coated dust particles then
17 react separately with trace gases.

18 19 **2.4 Simulations conducted**

20 Eleven simulations were conducted (Table 2) to examine the impact of the dust storm on
21 tropospheric chemistry. No_Dust serves as a base simulation in which heterogeneous chemistry
22 on dust surfaces and the effect of dust on photolysis rates are not included. Dust_J simulation
23 includes the effect of dust aerosols on photolysis rates, while Dust_JH simulation is same as

1 Dust_J but with addition of heterogeneous chemistry on dust surface taking into account the RH
2 dependence of γ and renoxification process. Dust_JH_NoRH simulation is same as Dust_JH
3 except that it does not include the RH dependence of γ . In Dust_JH_NoReNOx, the release of
4 gas-phase NO₂ associated with uptake of HNO₃ is excluded in order to assess the importance of
5 the renoxification process. Dust_JH_LoG and Dust_JH_HiG simulations are conducted with
6 lower and upper bounds of γ reported in the literature in order to provide an estimate of the
7 uncertainty in heterogeneous chemistry induced changes in tropospheric chemistry due to the
8 uncertainty in γ . Dust_JH_NO₃ and Dust_JH_SO₄ simulations are designed to examine the
9 influences of dust coated with nitrate and sulfate separately on the uptake of O₃. In these
10 simulations, the uptake coefficient γ for aged dust particles is reduced by 70% in Dust_JH_NO₃
11 and is increased by 33% in Dust_JH_SO₄ (Usher et al., 2003). Dust particles are coated with
12 both sulfate and nitrate in Dust_JH_NO₃_SO₄ to examine the combined effect of nitrate and
13 sulfate coating on O₃ uptake. In this simulation, three reactions of O₃ are included: with fresh
14 dust particles, dust particles coated with nitrate and dust particles coated with sulfate. The
15 original γ value is used for reaction with fresh dust particles, while the original γ value is reduced
16 by 70% for reaction with dust particles coated with nitrate and is increased by 33% for reaction
17 with dust particles coated with sulfate. Dust_JH_Sat is a hypothetical simulation where we
18 assume that the presence of a nitrate or sulfate monolayer on the dust particle would saturate the
19 dust particles and deactivate them for further catalytic uptake of O₃, OH, HO₂, H₂O₂,
20 CH₃COOH, CH₃OH and HCHO, but the coating is assumed to have no effect on the uptake of
21 HNO₃, NO₂, NO₃, N₂O₅ and SO₂. This comparison of Dust_JH_Sat with Dust_JH and Dust_J
22 would provide bounds of the heterogeneous chemistry induced changes in tropospheric
23 chemistry.

1
2
3
4
5
6
7
8
9
10
11
12
13
14
15
16
17
18
19

3. Observation datasets

3.1 Surface observations

This study uses surface O₃ and NO_y (sum of nitrogen oxides) observations made at the high altitude site Nainital (79.45°E, 29.36°N, 1958 m amsl) located in the central Himalayas. The observation site is bounded by high altitude (2-5 km) mountains in the North and East directions and opens to the Indo-Gangetic Plain region in the South and West directions. There are no major anthropogenic sources near Nainital and thus the observations at this site are envisaged to be representative of northern India (Kumar et al., 2010). Further details regarding the orography, vegetation cover, meteorological and chemical characteristics of Nainital can be found elsewhere (e.g. Sagar et al., 2004; Pant et al., 2006; Kumar et al., 2010; Sarangi et al., 2014). Ozone measurements are made using a standard ultraviolet absorption based instrument, and NO_y measurements are made with a chemiluminescence-based instrument. More details about the measurement set-up, operating principle, accuracy, detection limits and calibration procedure are discussed elsewhere (e.g. Kumar et al., 2010; Sarangi et al., 2014). The model results are also compared with Aerosol Robotic Network (AERONET) measurements at seven sites in the model domain. Further details of AERONET and these observations sites can be found in Kumar et al. (2014).

3.2 Ozone Monitoring Instrument (OMI)

The Ozone Monitoring Instrument (OMI), aboard NASA's Earth Observing System (EOS) Aura satellite, measures the radiation backscattered by the Earth's atmosphere and surface over the 0.27-0.5 μm wavelength range with a spatial resolution of about 13 km x 24 km at nadir in

1 normal operational mode. These measured radiances are used for daily global retrievals of
2 several trace species, such as O₃, NO₂, BrO, SO₂, CH₂O and aerosols. However, we do not use
3 OMI O₃ and SO₂ retrievals because of their low sensitivity in the lower troposphere, which is the
4 region of interest in this study. We find that OMI SO₂ retrievals are very noisy as average OMI
5 retrieved SO₂ planetary boundary layer (PBL) column amount values (0.5-1.0 DU) are smaller
6 than the reported standard deviation of the noise (1.5 DU). Here, we use Level-2 tropospheric
7 column NO₂ datasets made available by KNMI (Royal Netherlands Meteorological Institute) as
8 they provide access to the averaging kernel and a priori profiles, which are needed to make a
9 proper comparison between model profiles and satellite retrievals (e.g. Emmons et al., 2004).
10 More details on the algorithm used to retrieve the tropospheric column NO₂ abundances at
11 KNMI are described by Bucsela et al. (2006). These OMI NO₂ retrievals were found to correlate
12 well with aircraft measurements made during the INTEX-B campaign (Boersma et al., 2008) and
13 MAX-DOAS ground-based measurements (Kramer et al., 2008) but are also suggested to be
14 biased positively by about 0-30%, irrespective of season (e.g. Boersma et al., 2009a; Zhou et al.,
15 2009).

16

17 To compare WRF-Chem results with OMI, the best quality OMI retrievals are used by reducing
18 influence of clouds on OMI retrievals through selection of pixels with cloud fraction less than
19 0.3 and removing unreliable retrievals associated with a tropospheric column flag of greater than
20 0 (Boersma et al., 2009b). The nighttime pixels from OMI are also excluded for the comparison.
21 These best quality retrievals are co-located in space and time with model output. The co-located
22 WRF-Chem profiles are then transformed using the averaging kernel and a priori profiles used in
23 the satellite retrievals to obtain a model profile that OMI would measure for the modeled state of

1 the atmosphere in the absence of other errors. More details about the method of model-OMI data
2 co-location and convolution of model profiles with averaging kernel and a priori files can be
3 found in Kumar et al. (2012).

4

5 **4. Results and Discussion**

6 **4.1 Model Evaluation**

7 Dust storms in northern India are characterized by large increase in AOD (>50%) and decrease
8 in α (>70%) (Dey et al., 2004, Prasad and Singh, 2007). Both of these features were observed
9 during this dust storm indicating that this was a typical pre-monsoon season dust storm (see
10 Kumar et al., 2014) and can be considered as representative of dust storms in northern India.
11 Kumar et al. (2014) also present a detailed evaluation of simulated aerosol optical properties and
12 here, we present a summary. The simulated aerosol optical depth (AOD), Angström exponent
13 and single scattering albedo are compared against Aerosol Robotic Network (AERONET)
14 measurements at seven sites in the model domain. It is found that the model generally
15 underestimates the AOD over the model domain but is able to capture the temporal variations (r
16 = 0.5-0.88) seen in AERONET measurements. The good agreement between modeled and
17 AERONET observed Angström exponent indicates that the model is able to capture dust storm-
18 induced variations in aerosol size. The comparison of model results with Moderate Resolution
19 Imaging Spectroradiometer (MODIS) AOD retrievals shows that the model is also able to
20 capture the spatial pattern of dust storm induced changes in the MODIS AOD as well as the
21 spatial pattern of the dust plume. The average MODIS and WRF-Chem AOD (550 nm) values in
22 the high dust laden region are estimated as 0.80 ± 0.30 and 0.68 ± 0.28 respectively.

23

1 The variations in observed and WRF-Chem simulated (No_Dust, Dust_J, Dust_JH_NoRH and
2 DUST_JH) daily average O₃ and NO_y at Nainital during 13-24 April 2010 are shown in Figure 2.
3 The modeled time series of relative humidity and dust mass concentration for particles of 0.73,
4 1.4 and 8.0 μm effective radii at Nainital are also shown. Note that the WRF-Chem model at the
5 resolution (30 x 30 km²) used here is not able to capture the rapidly varying topography around
6 Nainital and the altitude of the site in the model is off by about 900 m. To minimize the
7 comparison errors induced by this spatial mismatch, we first obtain the altitude profile of model
8 results at Nainital by bi-linearly interpolating model output at each model level to the location of
9 Nainital (79.45°E, 29.36°N) and then linearly interpolate the resulting altitude profile to the
10 height of Nainital (1958 m). Dust mass concentrations started increasing at Nainital on 17 April
11 2010, reached a maximum during 20-22 April and decreased thereafter. The mass concentrations
12 of 8.0 μm particles remain close to zero even during the dust storm because these particles do not
13 travel far from the source regions due to their higher deposition velocities resulting in dry
14 deposition.

15
16 The observed O₃ mixing ratios show a decrease during the dust storm period (17-22 April 2010),
17 while observed NO_y mixing ratios show an increase during 17-18 April 2010 and a decrease
18 thereafter. Analysis of back-air trajectories arriving at Nainital (not shown) showed that the
19 increase in NO_y levels at Nainital during 17-18 April was associated with passage of low altitude
20 air masses over the Indo-Gangetic Plain region before arriving at Nainital, while air masses on
21 previous days (15-16 days) passed over relatively cleaner regions to the north and west at higher
22 altitudes. The WRF-Chem model without incorporating the effects of dust aerosols (No_Dust)
23 does not capture the observed decrease in O₃ and NO_y levels at Nainital. Including effects of dust

1 on photolysis rates (Dust_J) induces a slight decrease (about 2 ppbv) in modeled O₃ levels, but
2 modeled values are still significantly higher than the observations. The introduction of
3 heterogeneous chemistry without including RH dependence of γ (Dust_JH_NoRH) in the model
4 leads to the observed decreases in O₃ and NO_y, but compared to measurements we find too strong
5 of decreases in O₃ levels and slightly higher NO_y levels than the observations at Nainital during
6 the peak of dust storm, i.e. 20-22 April 2010. The inclusion of heterogeneous chemistry with RH
7 dependence of γ (Dust_JH) leads to the best agreement between WRF-Chem simulated and
8 observed O₃ and NO_y values at Nainital. The WRF-Chem simulated average O₃ values at
9 Nainital in Dust_JH and No_Dust configurations during 17-22 April 2010 are estimated to be
10 58 ± 5 ppbv and 73 ± 6 ppbv respectively as compared to the average observed value of 56 ± 10
11 ppbv. The corresponding WRF-Chem NO_y average values at Nainital are estimated as 1189 ± 751
12 pptv and 2945 ± 876 pptv, respectively, as compared to the average observed value of 843 ± 887
13 pptv. Thus, including the effects of dust aerosols in WRF-Chem reduces the difference between
14 average modeled and observed O₃ from 16 ± 9 to 2 ± 8 ppbv and that in NO_y from 2102 ± 1425 to
15 346 ± 1225 pptv respectively.

16

17 The spatial distributions of average OMI retrieved and WRF-Chem (Dust_JH and No_Dust)
18 simulated tropospheric column NO₂ during 13-16 April 2010 and 17-22 April 2010 are shown in
19 Figure 3. The percentage differences in tropospheric column NO₂ between high and low dust
20 emission periods are also shown for both OMI and WRF-Chem. Both the model and satellite
21 data show similar spatial distributions with the highest values along the Indo-Gangetic Plain
22 region during both low and high dust emission periods, but WRF-Chem generally overestimates
23 the OMI retrievals which is consistent with previous studies over the Indian region (Kumar et al.,

1 2012; Ghude et al., 2013). However, the comparison between Dust_JH and No_Dust
2 configurations of WRF-Chem shows that the inclusion of effects of dust aerosols improves the
3 model performance and reduces the model bias with respect to OMI retrievals by up to 30%
4 especially in the Indo-Gangetic Plain region. The remaining bias in the model could be due to
5 uncertainties in NO_x emission estimates in this region. The percentage difference plots show that
6 the WRF-Chem model is able to capture several features of changes in OMI retrieved spatial
7 distribution of tropospheric column NO₂ between high and low dust emission periods. The
8 domain averaged OMI and WRF-Chem (Dust_JH) tropospheric column NO₂ values over the
9 geographical region (70°-80°E, 25°-30°E) of maximum dust storm impact during low dust
10 emission period are estimated as $(2.35 \pm 1.43) \times 10^{15}$ and $(3.95 \pm 2.43) \times 10^{15}$ molecules cm⁻²
11 respectively, and during high dust emission period are estimated as $(2.01 \pm 1.37) \times 10^{15}$ and
12 $(3.41 \pm 2.80) \times 10^{15}$ molecules cm⁻² respectively. The reduction in tropospheric column NO₂
13 during high dust emission period in both OMI and WRF-Chem indicates that the dust storm
14 acted as a sink for NO₂.

15

16 **4.2 Impact of dust storm on photolysis rate coefficients**

17 The impact of the dust storm on photolysis rates is examined by comparing the daytime (0730-
18 1730 IST or 0200-1200 UTC) NO₂ photolysis rate coefficients calculated by the WRF-Chem
19 model with Dust_J and No_Dust configurations (Figure 4). NO₂ photolysis rates at the surface
20 show a strong relationship with aerosol loading and are lowest over the Indo-Gangetic Plain
21 region, which is where the anthropogenic emissions are stronger than those over other parts of
22 the model domain. The inclusion of dust aerosols enhances the spatial heterogeneity of NO₂
23 photolysis rate and decreases it by 5-25% over the Thar Desert and western Indo-Gangetic Plain

1 region. The photolysis rate coefficients of other trace gases such as O₃, HNO₃, H₂O₂, CH₂O and
2 N₂O₅ at the surface exhibit similar features (not shown) with decreases of the same order of
3 magnitude. The magnitude of change in photolysis rates decreases with altitude and changes sign
4 from negative to positive near 4 km because of the increase in actinic flux due to scattering of
5 incoming solar radiation by dust aerosol layers underneath. The spatial structure of changes in
6 photolysis rates at 100 hPa is similar to that at the surface with the largest increases (1-5%) over
7 the Thar Desert and western Indo-Gangetic Plain region.

8

9 **4.3 Impact of dust storm on trace gases at the surface**

10 To determine the impact of the dust storm on surface composition, average surface mixing ratios
11 of O₃, SO₂, NO_x, HNO₃ and H₂O₂ in the DUST_JH, which is the simulation that compared best
12 with observations at Nainital, and the No_Dust simulation are compared for the dust event time
13 period of 17-22 April 2010 (Figure 5). Surface O₃ shows a similar spatial distribution in both
14 runs with the lowest values over the Arabian Sea and the highest values over the eastern Indo-
15 Gangetic Plain region. However, the dust storm clearly leads to a reduction in O₃ mixing ratios
16 by 3-14 ppbv (5-25%) over the Thar Desert and western Indo-Gangetic Plain region. The spatial
17 distribution of reductions in O₃ mixing ratios is consistent with the distribution of dust over the
18 model domain and the amount of reduction is comparable to those reported by previous studies
19 in dust source regions (e.g. Dentener et al., 1996; Tang et al., 2004; Pozzoli et al., 2008; Wang et
20 al., 2012).

21

22 Sulfur dioxide and NO_x mixing ratios are highest along the Indo-Gangetic Plain region due to
23 higher emissions in this region (Figure 5). Changes in SO₂ mixing ratios show a mixed response

1 to heterogeneous chemistry with a decrease of 0.1-0.2 ppbv (8-10%) over the Thar Desert region
2 and an increase of 0.2-0.5 ppbv (2-6%) over the eastern Indo-Gangetic Plain region. This is
3 because the heterogeneous chemistry reduces SO_2 through reaction with dust particles while
4 increases it through reduction of OH mixing ratios ($\text{SO}_2 + \text{OH} \rightarrow \text{Sulfate}$). The sign of the
5 changes in SO_2 is thus determined by competition between these two reactions. In general, NO_x
6 mixing ratios show a reduction of up to 0.5 ppbv (<10%) along the Indo-Gangetic Plain region
7 and 0.2-0.3 ppbv (10-20%) over the Thar Desert due to uptake of NO_2 by dust particles. The
8 changes in NO_2 are also determined by the competition between the reactions of NO_2 with dust
9 and OH where the former tends to decrease NO_2 while the latter tends to increase NO_2 due to
10 reduced OH. The reduction in NO_x is in contrast with the results of Wang et al. (2012) who
11 reported an increase in NO_x in the dust source region and attributed the increase to the
12 renoxification process. Our study differs because Wang et al. (2012) assumed that renoxification
13 process is active all the time, whereas this process is active only during daytime in our
14 simulations. To quantify the contribution of renoxification process in the NO_x budget, we
15 compared the NO_x distributions simulated by Dust_JH and Dust_JH_NoReNOx configurations.
16 The comparison (not shown) showed that the renoxification process does increase NO_x mixing
17 ratios, but the magnitude of this increase (0.1-0.2 ppbv) is likely less than the reduction due to
18 heterogeneous chemistry.

19

20 The spatial distributions of HNO_3 and H_2O_2 (Figure 5) are largely modified by the dust storm
21 with reduction of up to 2 ppbv (~99%), because these species are highly reactive with dust
22 particles (Table 1). The large reduction in H_2O_2 mixing ratio estimated here is also in contrast
23 with the results of Wang et al. (2012) who estimated an increase in H_2O_2 . Wang et al. (2012)

1 assumed a 100% yield for the conversion of HO₂ into H₂O₂ through heterogeneous uptake, while
2 we assume a yield of 10% following recent work by Bedjanian et al. (2013b). Mixing ratios of
3 NO₃, N₂O₅ and CH₃COOH also show large reductions by Dust_JH with the highest decrease
4 reaching up to 0.1 ppbv (~98%), 0.46 ppbv (~99%) and 0.45 ppbv (~96%) respectively. The
5 uptake of HO₂ by dust particles leads to a maximum reduction of about 3.5 pptv (~40%) over the
6 Thar Desert region, which is much less than those reported previously (e.g. Bian and Zender,
7 2003; Wang et al., 2012) and is attributed to a lower γ value used in our study (<0.064 vs. 0.1).
8 The maximum reduction in OH, CH₂O and CH₃OH is estimated to be about 40%, 21% and 5%,
9 respectively.

10

11 The above discussion includes both the role of heterogeneous chemistry in changing the
12 distribution of trace gases however and dust-modified photolysis rate coefficients. The individual
13 contributions of heterogeneous chemistry and perturbation in photolysis rate coefficients to the
14 total difference in distributions of trace gases at the surface are estimated by comparing
15 differences between simulations (Figure 6). More than 80% of the changes in distribution of
16 these trace gases are explained by the heterogeneous chemistry. The changes in surface O₃
17 induced by dust-modified photolysis rate coefficients are within ± 1 -3 ppbv and are driven by the
18 complex response of O₃ to decreases in photolysis rate coefficients. A decrease in the photolysis
19 rate coefficients leads to slower photochemical processing in general and thus decreased O₃
20 production.

21

22 Mixing ratios of surface SO₂ and NO_x show an increase of up to 0.1 ppbv due to reduction in
23 photolysis rate coefficients. The increase in NO_x and SO₂ is associated with a decrease in OH

1 mixing ratios as reaction with OH is the main loss process for both NO_x and SO₂. The decrease
2 in O₃ photolysis rate coefficient leads to a decrease of up to 30% in OH (O₃ + hv → O¹D + O₂,
3 producing OH through reaction of O¹D with water vapor) mixing ratios. Mixing ratios of surface
4 HNO₃ and H₂O₂ also show a small decrease of up to 0.4 and 0.6 ppbv in the Dust_J
5 configuration relative to the No_Dust configuration. HNO₃ is produced mainly by the reaction of
6 OH with NO₂ but the rate of change of HNO₃ is dominated by changes in OH as the reduction in
7 OH (up to 30%) is larger than that in NO₂ (up to 5%). The reduction in H₂O₂ is also associated
8 with reduction in OH and HO₂ mixing ratios. Since OH is the major oxidizing agent in the
9 troposphere, a decrease in OH also leads to a decrease in the oxidizing capacity of the
10 atmosphere and a consequent increase of up to 5-10% in several trace gases such as CO, alkanes
11 and alkenes at the surface.

12

13 **4.4 Impact of dust storm on vertical distribution of trace gases**

14 In addition to changes in surface mixing ratios, vertical distributions of trace gases are modified
15 by the dust storm via heterogeneous chemistry and dust-modified photolysis rates. By averaging
16 over the region of maximum dust influence (70-80E, 25-30N) for each simulation, the
17 percentage differences between Dust_JH and No_Dust giving the total difference, Dust_J and
18 No_Dust giving the contribution of modified photolysis rates, and Dust_JH and Dust_J giving
19 the contribution from heterogeneous chemistry are found. Profiles of O₃, NO_x, HNO₃, OH and
20 BIGALK are shown in Figure 7. BIGALK represents alkanes with four or more carbon atoms in
21 the MOZCART chemical mechanism and is shown to illustrate the dust storm induced changes
22 in volatile organic compounds.

23

1 The changes in all the trace gases due to heterogeneous chemistry are much larger than those due
2 to perturbations in photolysis rate coefficients, and are significant below 8 km, which is
3 consistent with the vertical distribution of dust particles (Figure 7). All gases except BIGALK
4 show a net reduction because of the larger changes induced by the heterogeneous chemistry. The
5 reduction in OH due to decrease in O₃ photolysis rate coefficient leads to a small increase of 1-
6 4% in NO_x. The reaction with OH is the only loss process for BIGALK and therefore BIGALK
7 shows an increase due to both heterogeneous chemistry and perturbation in photolysis rates as
8 both of these processes leads to a decrease in OH. The highest net decrease in O₃, NO_x, HNO₃
9 and OH are estimated as ~16%, ~26%, ~91% and ~30% respectively while the highest net
10 increase in BIGALK is estimated as ~26%. The vertical distribution of changes in NO₃, N₂O₅,
11 H₂O₂ and CH₃COOH are similar to those in HNO₃ and the highest net reduction reaches 80-90%.

12

13 **4.5 Importance of RH dependence of reactive uptake coefficients (γ)**

14 The uptake of trace gases by dust aerosols also depends upon the relative humidity as reactive
15 uptake coefficients have a large variation with RH. The effect of relative humidity on the rate
16 constants k_{O_3} and k_{HNO_3} at the surface over the model domain during 17-22 April 2010 is
17 illustrated in Figure 8, where model runs with and without RH dependence of γ are compared.
18 The spatial distributions of average mass concentration for dust particles of 1.4 μm effective
19 radius and relative humidity are also shown to help the interpretation. RH is less than 20% over
20 most of the Indian region and is 70-90% over the oceanic regions. As expected, the spatial
21 distributions of both k_{O_3} and k_{HNO_3} in both configurations are nearly identical to the distribution
22 of dust mass concentrations with the highest values in the dust source regions. The rate constant

1 decreases for O_3 while increases for HNO_3 by one-two orders of magnitude after inclusion of RH
2 dependence of γ . The rate coefficients for other gases show a similar spatial distribution.

3
4 The effect of RH induced changes in the rate constants on heterogeneous uptake of O_3 , SO_2 ,
5 HNO_3 , H_2O_2 , OH and HO_2 is illustrated by showing the relative percentage differences in the
6 distribution of these gases in the lowest model layer between the model runs with and without
7 RH dependence of γ (Figure 9). Surface O_3 and HO_2 show an increase when RH effects on γ are
8 included because γ for these gases decrease with RH. In contrast, HNO_3 and H_2O_2 uptake
9 coefficients increase when RH effects are accounted for, resulting in a decrease in HNO_3 and
10 H_2O_2 mixing ratios. The changes in O_3 , HO_2 and H_2O_2 reach up to 20%, 25% and 50%,
11 respectively, over the Thar Desert and the western Indo-Gangetic Plain region. The percentage
12 changes in HNO_3 reach up to 100% and are higher over the oceanic regions ($RH > 45\%$) than the
13 inland regions because of the order of magnitude increase of γ for HNO_3 when RH increases
14 above 40%. Surface SO_2 and OH show a mixed response with increase over some parts of the
15 model domain and decrease over the others. The changes in SO_2 and OH are within $\pm 10\%$. The
16 changes in SO_2 are determined by the competition between the reactions of SO_2 with dust
17 particles and OH . The heterogeneous reaction of SO_2 tries to reduce SO_2 due to increase in γ
18 with RH while that with OH would decrease (increase) SO_2 if OH increases (decreases). The
19 magnitudes of these RH induced changes in trace gases are comparable to those induced by
20 heterogeneous chemistry (reported in section 4.3). This suggests that consideration of RH
21 dependent γ values in heterogeneous chemistry calculations is as important as is the accurate
22 simulation of dust mass concentrations.

23

1 **4.6 Effect of uncertainty in reactive uptake coefficient (γ)**

2 The effect of uncertainty in reactive uptake coefficient (γ) on heterogeneous chemistry induced
3 changes in the tropospheric chemistry are illustrated in Figure 10, where model runs with lower
4 (Dust_JH_LoG) and upper (Dust_JH_HiG) bounds of γ are compared in the lowest model layer.
5 It is clear that uncertainty in γ can lead to significant uncertainty in heterogeneous chemistry
6 induced changes in all gases. Surface O₃ mixing ratios have uncertainties of up to 8-11 ppbv (25-
7 30%), while other gases have uncertainties of up to 1-1.5 ppbv (30-100%), except SO₂ and NO₂,
8 which show uncertainties of up to 3 ppbv (30-70%) at some locations. A comparison of these
9 uncertainties with the total change induced by dust storm in these gases (Figure 5 and section
10 4.3) reveal that uncertainties in O₃, HNO₃, NO₃, N₂O₅, OH, HO₂, H₂O₂, and CH₃COOH due to
11 the uptake values have magnitudes similar to the total changes induced by dust aerosols, while
12 those in NO₂, SO₂ and CH₃OH are even greater than the total changes induced by dust storm.
13 These results highlight the importance and necessity of accurate measurements of reactive uptake
14 coefficients.

15

16 **4.7 Impact of dust aging**

17 The aging of dust particles through heterogeneous uptake of gases can modify the dust reactivity
18 towards trace gases. We have made an attempt to simulate changes in the dust reactivity and
19 uptake of trace gases due to nitrate and sulfate coating and the results are presented in this
20 section. The spatial distributions of WRF-Chem simulated average mass concentration of fresh
21 and aged dust particles of 1.4 μm effective radius at the surface in Dust_JH_NO₃, Dust_JH_SO₄
22 and Dust_JH_NO₃_SO₄ configurations during 17-22 April 2010 are shown in Figure 11. In
23 general, fresh dust particles are seen mostly in and near the source regions because all dust

1 particles are emitted as fresh particles and have much smaller concentrations than the aged dust
2 particles particularly outside the dust source regions. Among all the gases providing nitrate
3 coating on dust particles, the HNO_3 uptake makes the highest contribution to the concentration of
4 aged particles due to its higher mixing ratios and strong increase in its reactivity towards the dust
5 surface with relative humidity. For example, if there are 10 fresh dust particles cm^{-3} of effective
6 radius $0.73 \mu\text{m}$, then the uptake of HNO_3 , NO_2 , NO_3 and N_2O_5 leads to about 2.5 aged dust
7 particles cm^{-3} in one time step (180 s) at $\text{RH} = 0$, and HNO_3 and NO_3 each provide about 1 dust
8 particle. However, the number concentration of aged dust particles formed due to HNO_3 uptake
9 increases to about 7 particles cm^{-3} per time step as RH increase to 20-40%. The uptake of SO_2
10 also increases with increase in relative humidity, but the SO_2 contribution to the aged particles is
11 much less than that of HNO_3 due to lower SO_2 γ values. The decrease in O_3 γ values for nitrate
12 coated dust particles leads to an enhancement of 1-2 ppbv in surface O_3 over the Thar Desert and
13 western Indo-Gangetic Plain region relative to uncoated dust particles (Figure 11) while increase
14 in O_3 γ values for sulfate coated dust particles leads to a reduction of 0.5-1 ppbv over these
15 regions. Since nitrate coating leads to a larger fraction of aged particles than the sulfate coating,
16 surface O_3 mixing ratios show an overall enhancement of up to 1 ppbv over the regions of high
17 dust loadings when both sulfate and nitrate coated dust particles are allowed to react with O_3 in
18 the model.

19

20 The presence of a nitrate or sulfate monolayer on the dust particle might saturate the dust
21 particles and deactivate them for further catalytic uptake of other gases. In order to examine the
22 effect of such a coating on the uptake of O_3 , H_2O_2 , HCHO and CH_3COOH , lower and upper
23 bounds of heterogeneous chemistry reaction rates induced changes in the surface mixing ratios of

1 these gases are calculated (Figure 12). Lower and upper bounds for each gas are calculated by
2 subtracting their average values in Dust_J configuration from those in Dust_JH and Dust_JH_Sat
3 configurations respectively. Absolute mixing ratios of these gases in Dust_J configuration, in
4 which dust aerosols affected photolysis rates only, are also shown to provide an idea of the
5 modification in base levels of these gases due to heterogeneous chemistry. As expected, the
6 saturation of dust particles decreases the magnitude of reduction caused by heterogeneous
7 chemistry for all the gases by 5-50%. The amount of maximum reduction in surface O₃ changed
8 from 20-25% to 15-20% when saturation effects are accounted for. The saturation of dust
9 particles has a larger impact on the distribution of H₂O₂ and CH₃COOH as maximum reduction
10 in both of these gases decreased to 20-40% (as compared to 70-90% for unsaturated dust
11 particles) over the Thar Desert and dust source regions. Both of these gases show a small
12 increase of 0.1-0.2 ppbv (less than 10%) outside the source regions for the case of saturated dust
13 particles. The maximum reduction in HO₂ and OH (not shown) also changes from 20-40% in
14 Dust_JH to 5-20% in Dust_JH_Sat. Some changes can also be discerned in the distribution of
15 HCHO and CH₃OH (not shown) but they are within ±5%.

16

17 **5. Summary**

18 The effects of a typical pre-monsoon season dust storm on tropospheric chemistry are analyzed
19 for a case study in northern India, using the Weather Research and Forecasting model coupled
20 with Chemistry (WRF-Chem), which is further developed to enhance its ability to simulate
21 tropospheric chemistry in the presence of dust particles. The changes made to the model are
22 specific to the MOZCART setup. Two major updates are included in this study: firstly, the F-
23 TUV photolysis scheme of the model is updated to include the effect of dust aerosols on

1 photolysis rates and to achieve consistency between the methods through which aerosols affect
2 the meteorology and photolysis rates in the model. Secondly, a new scheme consisting of twelve
3 heterogeneous reactions is included to simulate heterogeneous chemistry on the surface of dust
4 particles. The relative humidity dependence of uptake coefficients, which was ignored in most
5 previous studies, is used for six of the heterogeneous reactions.

6

7 The extended configuration of WRF-Chem is applied to a typical pre-monsoon season dust storm
8 that occurred in northern India during 17-22 April 2010. The model reproduced the spatial and
9 temporal distribution of dust plumes and aerosol optical properties (Kumar et al., 2013). The
10 simulations are evaluated against surface O_3 and NO_y observations at a high altitude (1958 m)
11 measurement station in the Himalayan region (Nainital), and the model is found to capture the
12 observed decrease in O_3 and NO_y during the dust storm only after the inclusion of the effects of
13 dust on photolysis rates and heterogeneous chemistry. Average observed and modeled O_3 values
14 at Nainital during 17-22 April 2010 are estimated to be 56 ± 10 and 58 ± 5 ppbv respectively, and
15 the corresponding NO_y values are estimated to be 843 ± 887 and 1189 ± 751 pptv respectively. The
16 extended configuration of the model also reduced biases in tropospheric column NO_2 by up to
17 30% compared to OMI retrievals and captured the general features of the dust storm induced
18 changes in the spatial distribution of OMI-retrieved tropospheric column NO_2 .

19

20 Several sensitivity simulations are conducted to investigate the contribution of different
21 processes on mixing ratios of several key trace gases including ozone, nitrogen oxides, hydrogen
22 oxides, methanol, acetic acid and formaldehyde. The dust storm leads to a decrease of 5-25% in
23 photolysis rate coefficients of O_3 , NO_2 and other trace gases at the surface and an increase of 1-

1 5% above 4 km. It is found to have a significant impact on the regional tropospheric chemistry: a
2 decrease of 5-99% is estimated in the mixing ratios of a variety of trace gases including O₃,
3 nitrogen oxides, hydrogen oxides, sulfur dioxide, methanol, acetic acid and formaldehyde at the
4 surface. Analysis of the vertical distributions of these trace gases shows that dust storm induced
5 changes are significant up to an altitude 8 km and are estimated as 80-90% (5-10 times) for
6 highly reactive gases such as HNO₃, NO₃, N₂O₅, H₂O₂ and CH₃COOH. It is found that the
7 majority of these changes are induced by the heterogeneous chemistry, while the contribution of
8 dust-modified photolysis rates generally remained less than 10%. An increase of up to 30% in
9 volatile organic compounds is estimated due to decreases in OH concentrations.

10

11 The RH dependence of γ is found to play a large potential role in heterogeneous chemistry.
12 Sensitivity studies showed that the exclusion of the RH dependence can introduce a difference of
13 one-two orders of magnitude in heterogeneous reactions rate constants, 20-25% changes in O₃
14 and HO₂, and up to 50% and 100% changes in H₂O₂ and HNO₃, respectively. These effects are
15 comparable to heterogeneous chemistry induced changes in these gases. The effect of
16 uncertainties in the uptake coefficients (γ) on the distribution of trace gases is examined using
17 sensitivity simulations with lower and upper bounds of γ . Differences of trace gas mixing ratios
18 caused by uncertainties in the uptake coefficients are found to be the same magnitude or greater
19 as the differences in mixing ratios induced by dust storm effects on tropospheric chemistry. We
20 also tested the importance of atmospheric aging of dust particles in the context of heterogeneous
21 chemistry. Model experiments based on laboratory studies of changes in dust reactivity due to
22 atmospheric aging showed that coating of dust with nitrate and sulfate may lead to changes of up
23 to 1 ppbv in surface O₃ simulations. A hypothetical simulation is also conducted by saturating

1 the nitrate and sulfate coated dust particles for uptake of O_3 , HO_2 , OH , H_2O_2 , CH_3COOH ,
2 CH_3OH and $HCHO$. The saturation of dust particles is found to have a larger impact on the
3 distributions of H_2O_2 and CH_3COOH but a relatively small impact on other gases.

4
5 This study clearly shows that the pre-monsoon season dust storm can potentially affect the
6 regional tropospheric chemistry in northern India. However, the implications of the
7 heterogeneous uptake of trace gases on aerosol size distributions and their feedbacks on the
8 radiation budget and cloudiness are not examined here. Dust particles coated with nitrate/sulfate
9 may interact differently with radiation as compared to uncoated dust particles and can increase or
10 decrease cloudiness depending upon their size distribution. Both of these processes will have
11 important implications for the direct aerosol radiative forcing and the Elevated Heat Pump (EHP)
12 hypothesis (Lau et al., 2006), which proposed that the absorption of solar radiation by dust and
13 black carbon aerosols along the southern slopes of Himalayas modulates the meridional
14 temperature gradient and leads to an early onset of Indian summer monsoon. The heterogeneous
15 chemistry scheme implemented in the MOZCART chemical mechanism here can be easily
16 extended to a more detailed aerosol module (e.g. MOSAIC) of WRF-Chem, which would allow
17 studies on the implications of heterogeneous chemistry for aerosols and their interaction with
18 radiation, clouds, and the Asian monsoon, including the role of aerosol aging on aerosol and
19 trace gas distributions.

20
21 Nevertheless, this study demonstrates that the effects of dust aerosols through heterogeneous
22 chemistry and perturbation in photolysis rates should be included in atmospheric chemistry
23 transport models, especially for simulating air quality in northern India. Although this study

1 analyzed a typical dust storm in northern India but more such studies should be conducted in
2 future to lend further confidence in these results. At the same time, it is also imperative to
3 improve the accuracy and precision of the reactive uptake coefficients, their dependence on
4 relative humidity and atmospheric processing of dust particles. In addition, extensive efforts
5 must be made to conduct co-located measurements of O₃ and related gases, along with physical
6 and chemical properties of dust aerosols in northern India, especially during the dust storm
7 season, to gain insights into the effects of dust aerosols on tropospheric chemistry and provide
8 more data for model evaluation.

9

10 **Acknowledgements**

11 We thank L. Emmons and C. Wiedinmyer for their constructive suggestions on the manuscript.
12 The datasets of initial and boundary conditions for meteorological fields were made available by
13 the NCAR research data archive (<http://rda.ucar.edu/datasets/ds083.2/>). The datasets for initial
14 and boundary conditions for chemical fields, biogenic emissions, biomass burning emissions,
15 and programs used to process these data sets were made available by the NCAR Atmospheric
16 Chemistry Division (<http://www.acd.ucar.edu/wrf-chem/>). We thank the OMI science team at
17 KNMI for providing tropospheric NO₂ retrievals. The National Center for Atmospheric Research
18 is supported by the National Science Foundation. Observations at Nainital are supported by
19 ISRO-ATCTM project. Comments from the two reviewers are greatly appreciated.

References

- 1
- 2 Bauer, S. E., Balkanski, Y., Schulz, M., Hauglustaine, D. A., and Dentener, F.: Global modeling
3 of heterogeneous chemistry on mineral aerosol surfaces: Influence on tropospheric ozone
4 chemistry and comparison to observations, *J. Geophys. Res.*, 109, D02304, doi:
5 10.1029/2003JD003868, 2004.
- 6 Bedjanian, Y., Romanias, M. N., and El Zein, A.: Interaction of OH Radicals with Arizona Test
7 Dust: Uptake and Products, *J. Phys. Chem. A*, 117 (2), 393-400, doi: 10.1021/jp311235h,
8 2013a.
- 9 Bedjanian, Y., Romanias, M. N., and El Zein, A.: Uptake of HO₂ radicals on Arizona test dust
10 surface, *Atmos. Chem. Phys. Discuss.*, 13, 8873-8900, doi: 10.5194/acpd-13-8873-2013,
11 2013b.
- 12 Beljaars, A.C.M.: The parameterization of surface fluxes in large-scale models under free
13 convection. *Quart. J. Roy. Meteor. Soc.*, **121**, 255–270 1994.
- 14 Bian, H. and Zender, C. S.: Mineral dust and global tropospheric chemistry: Relative roles of
15 photolysis and heterogeneous uptake, *J. Geophys. Res.*, 108, 4672,
16 doi:10.1029/2002JD003143, 2003.
- 17 Boersma, K. F., Dirksen, R. J., Veeffkind, J. P., Eskes, H. J., and van der A, R. J.: Dutch OMI
18 NO₂ (DOMINO) data product, HE5 data file user manual, <http://www.temis.nl/docs/OMI>
19 NO₂ HE5 1.0.2.pdf, 2009b.
- 20 Boersma, K. F., Jacob, D. J., Bucselá, E. J., Perring, A. E., Dirksen, R., vander A, R. J.,
21 Yantosca, R. M., Park, R. J., Wenig, M. O., Bertram, T. H., and Cohen, R. C.: Validation of
22 OMI tropospheric NO₂ observations during INTEX-B and application to constrain NO_x

1 emissions over the eastern United States and Mexico, *Atmos. Environ.*, 42, 4480–4497,
2 2008.

3 Boersma, K. F., Jacob, D. J., Trainic, M., Rudich, Y., DeSmedt, I., Dirksen, R., and Eskes, H. J.:
4 Validation of urban NO₂ concentrations and their diurnal and seasonal variations observed
5 from the SCIAMACHY and OMI sensors using in situ surface measurements in Israeli cities,
6 *Atmos. Chem. Phys.*, 9, 3867–3879, doi:10.5194/acp-9-3867-2009, 2009a.

7 Bucsela, E. J., Celarier, E. A., Wenig, M. O., Gleason, J. F., Veefkind, J. P., Boersma, K. F., and
8 Brinksma, E. J.: Algorithm for NO₂ vertical column retrieval from the ozone monitoring
9 instrument, *IEEE T. Geosci. Remote*, 44, 1245–1258, 2006.

10 Chen, F. and Dudhia, J.: Coupling and advanced land surface hydrology model with the Penn
11 State-NCAR MM5 modelingsystem, Part I: Model implementation and sensitivity,
12 *Mon. Weather Rev.*, 129, 569–585, 2001.

13 Chen, H., Navea, J. G., Young, M. A., and Grassian, V.H.: Heterogeneous Photochemistry of
14 Trace Atmospheric Gases with Components of Mineral Dust Aerosol. *J. Phys. Chem. A*, 115,
15 490–499, 2011.

16 Chin, M., Ginoux, P., Kinne, S., Holben, B. N., Duncan, B. N., Martin, R. V., Logan, J. A.,
17 Higurashi, A., and Nakajima, T.: Tropospheric aerosol optical thickness from the GOCART
18 model and comparisons with satellite and sunphotometer measurements, *J. Atmos. Sci.*, 59,
19 461-483, 2002.

20 Crowley, J. N., Ammann, M., Cox, R. A., Hynes, R. G., Jenkin, M. E., Mellouki, A., Rossi, M.
21 J., Troe, J., and Wallington, T. J.: Evaluated kinetic and photochemical data for atmospheric
22 chemistry: Volume V – heterogeneous reactions on solid substrates, *Atmos. Chem. Phys.*, 10,
23 9059-9223, doi:10.5194/acp-10-9059-2010, 2010.

1 Cwiertny, D. M., Young, M. A., and Grassian, V. H.: Chemistry and photochemistry of mineral
2 dust aerosol, *Annu. Rev. Phys. Chem.*, 59:27-51. doi:
3 10.1146/annurev.physchem.59.032607.093630, 2008.

4 DeFries, R. S., and Townshend, J. R. G.: NDVI-derived land cover classification at a global
5 scale, *Int. J. Remote Sens.*, 15, 3567-3586, 1994.

6 Dentener, F. J., Carmichael, G. R. , Zhang, Y., Lelieveld, J., and Crutzen, P. J.: Role of mineral
7 aerosol as a reactive surface in the global troposphere, *J. Geophys. Res.*, 101, 22869–22889,
8 1996.

9 Dey, S., Tripathi, S. N., Singh, R. P., and Holben, B. N.: Influence of dust storms on aerosol
10 optical properties over the Indo-Gangetic basin, *J. Geophys. Res.*, 109, D20211,
11 doi:[10.1029/2004JD004924](https://doi.org/10.1029/2004JD004924), 2004.

12 Emmons, L. K., Deeter, M. N., Gille, J. C., Edwards, D. P., Attié, J.-L., Warner, J., Ziskin, D.,
13 Francis, G., Khattatov, B., Yudin, V., Lamarque, J.-F., Ho, S.-P., Mao, D., Chen, J. S.,
14 Drummond, J., Novelli, P., Sachse, G., Coffey, M. T., Hannigan, J. W., Gerbig, C.,
15 Kawakami, S., Kondo, Y., Takegawa, N., Schlager, H., Baehr, J., and Ziereis, H.: Validation
16 of Measurements of Pollution in the Troposphere (MOPITT) CO retrievals with aircraft in
17 situ profiles, *J. Geophys. Res.*, 109, D03309, doi:10.1029/2003JD004101, 2004.

18 Emmons, L. K., Walters, S., Hess, P. G., Lamarque, J.-F., Pfister, G. G., Fillmore, D., Granier,
19 C., Guenther, A., Kinnison, D., Laepple, T., Orlando, J., Tie, X., Tyndall, G., Wiedinmyer,
20 C., Baughcum, S. L., and Kloster, S.: Description and evaluation of the Model for Ozone and
21 Related chemical Tracers, version 4 (MOZART-4), *Geosci. Model Dev.*, 3, 43-67,
22 doi:10.5194/gmd-3-43-2010, 2010.

1 Fast, J. D, Gustafson Jr., W. I., Easter, R. C., Zaveri, R. A., Barnard, J. C., Chapman, E. G., and
2 Grell, G. A.: Evolution of ozone, particulates, and aerosol direct forcing in an urban area
3 using a new fully-coupled meteorology, chemistry, and aerosol model, *J. Geophys. Res.*, 111,
4 D21305, doi: 10.1029/2005JD006721, 2006.

5 Freitas, S. R., Longo, K. M., Chatfield, R., Latham, D., Silva Dias, M. A. F., Andreae, M. O.,
6 Prins, E., Santos, J. C., Gielow, R., and Carvalho Jr., J. A.: Including the sub-grid scale
7 plume rise of vegetation fires in low resolution atmospheric transport models, *Atmos. Chem.*
8 *Phys.*, 7, 3385-3398, doi:10.5194/acp-7-3385-2007, 2007.

9 Ghude, S. D., Pfister, G. G., Jena, C., van der A, R. J., Emmons, L. K., and Kumar, R.: Satellite
10 constraints of nitrogen oxide (NO_x) emissions from India based on OMI observations and
11 WRF-Chem simulations, *Geophys. Res. Lett.*, 40, doi: 10.029/2012GL053926, 2013.

12 Ginoux, P., Chin, M., Tegen, I., Prospero, J. M., Holben, B., Dubovik, O., and Lin, S. J.: Sources
13 and distributions of dust aerosols simulated with the GOCART model, *J. Geophys. Res.-*
14 *Atmos.*, 106(D17), 20255–20273, 2001.

15 Goodman, A. L., Underwood, G. M., and Grassian, V. H.: A laboratory study of the
16 heterogeneous reaction of nitric acid on calcium carbonate particles, *J. Geophys. Res.*, 105,
17 29053–29064, 2000.

18 Granier, C. Bessagnet, B., Bond, T., D’Angiola, A., van der Gon, H. G., Frost, G. J., Heil, A.,
19 Kaiser, J. W., Kinne, S., Klimont, Z., Kloster, S., Lamarque, J.-F., Liousse, C., Masui, T.,
20 Meleux, F., Mieville, A., Ohara, T., Raut, J.-C., Riahi, K., Schultz, M. G., Smith, S. J.,
21 Thompson, A., van Aardenne, J., van der Werf, G. R. and van Vuuren, D. P.: Evolution of
22 anthropogenic and biomass burning emissions of air pollutants at global and regional scales

1 during the 1980–2010 period. , *Climate Change* 109 (1-2) : 163-190, doi: 10.1007/s10584-
2 011-0154-1, 2011.

3 Grassian, V. H.: Chemical reactions of nitrogen oxides on the surface of oxide, carbonate, soot,
4 and mineral dust particles: implications for the chemical balance of the troposphere, *J. Phys.*
5 *Chem. A*, 106, 860-877, doi: 10.1021/jp012139h, 2002.

6 Grell, G. A., Peckham, S. E., Schmitz, R., McKeen, S. A., Frost, G., Skamarock, W. C., and
7 Eder, B.: Fully coupled “online” chemistry within the WRF model, *Atmos. Environ.*, 39,
8 6957–6975, 2005.

9 Guenther, A., Karl, T., Harley, P., Wiedinmyer, C., Palmer, P. I., and Geron, C.: Estimates of
10 global terrestrial isoprene emissions using MEGAN (Model of Emissions of Gases and
11 Aerosols from Nature), *Atmos. Chem. Phys.*, 6, 3181-3210, doi:10.5194/acp-6-3181-2006,
12 2006.

13 Hatch, D. C., Gierlus, K. M., Schuttlefeld, J. D., and Grassian, V. H.: Water adsorption and
14 cloud condensation nuclei activity of calcite and calcite coated with model humic and fulvic
15 acids, *Atmos. Environ.*, 42 (22), 5672-5684, 2008.

16 Haywood, J. and Boucher, O.: Estimates of the direct and indirect radiative forcing due to
17 tropospheric aerosols: a review, *Reviews of Geophysics*, 38, 513–543, 2000.

18 Hegde, P., Pant, P., Naja, M., Dumka, U. C., and Sagar, R.: South Asian dust episode in June
19 2006: Aerosol observations in the central Himalayas, *Geophys. Res. Lett.*, 34, L23802, doi:
20 10.1029/2007GL030692, 2007.

21 Heikes, B. G. and Thompson, A. M.: Effects of heterogeneous processes on NO₃, HONO and
22 HNO₃ chemistry in the troposphere, *J. Geophys. Res.*, 88, 10883–10895, 1983.

1 Hodzic, A., Bessagnet, B., Vautard, R.: A model evaluation of coarse-mode nitrate
2 heterogeneous formation on dust particles, *Atmos. Environ.*, 40 (22), 4158-4171, 2006.

3 Hong, S.-Y., Yign N., Dudhia, J.: A new vertical diffusion package with an explicit treatment of
4 entrainment processes. *Mon. Wea. Rev.*, 134, 2318–2341, 2006.

5 Jacobson, M. Z.: *Fundamentals of Atmospheric Modeling*, 2nd edition, Cambridge University
6 Press, 2005.

7 Jickells, T. D., An, Z. S., Andersen, K. K., Baker, A. R., Bergametti, G., Brooks, N., Cao, J. J.,
8 Boyd, P. W., Duce, R. A., Hunter, K. A., Kawahata, H., Kubilay, N., laRoche, J., Liss, P.S.,
9 Mahowald, N., Prospero, J. M., Ridgwell, A. J., Tegen, I., and Torres, R.: Global iron
10 connections between desert dust, ocean biogeochemistry and climate, *Science*, 308, 67–71,
11 2005.

12 Kain, J. S.: The Kain-Fritsch convective parameterization: An update, *J. Appl. Meteor.*, 43, 170–
13 181, 2004.

14 Kelly, J. T., Chuang, C. C., and Anthony, S. W.: Influence of dust composition on cloud droplet
15 formation, *Atmos. Environ.*, 41, 2904–2904, 2007.

16 Kramer, L. J., Leigh, R., Remedios, J. J., and Monks, P. S.: Comparison of OMI and ground-
17 based in situ and MAX-DOAS measurements of tropospheric nitrogen dioxide in an urban
18 area, *J. Geophys. Res.*, 113, D16S39, doi: 10.1029/2007JD009168, 2008.

19 Kumar, R., Barth, M. C., Pfister, G. G., Naja, M., and Brasseur, G. P.: WRF-Chem simulations
20 of a typical pre-monsoon dust storm in northern India: influences on aerosol optical
21 properties and radiation budget, *Atmos. Chem. Phys.*, 14, 2431-2446, doi:10.5194/acp-14-
22 2431-2014, 2014.

1 Kumar, R., Naja, M., Pfister, G. G., Barth, M. C., Wiedinmyer, C., and Brasseur, G. P.:
2 Simulations over South Asia using the Weather Research and Forecasting model with
3 Chemistry (WRF-Chem): chemistry evaluation and initial results, *Geosci. Model Dev.*, 5,
4 619-648, doi:10.5194/gmd-5-619-2012, 2012.

5 Kumar, R., Naja, M., Venkataramani, S., and Wild O.: Variations in surface ozone at Nainital, a
6 high altitude site in the Central Himalayas, *J. Geophys. Res.*, 115, D16302, doi:
7 10.1029/2009JD013715, 2010.

8 Lau, K. M., Kim, M. K., and Kim, K. M.: Asian summer monsoon anomalies induced by aerosol
9 direct forcing: The role of the Tibetan Plateau, *Clim. Dyn.*, 26, 855-864, doi:
10 10.1007/s00382-006-0114-z, 2006.

11 Levin, Z., Ganor, E., and Gladstein, V.: The effects of desert particles coated with sulfate on rain
12 formation in the eastern Mediterranean, *J. Appl. Meteor.*, 35, 1511–1523, 1996.

13 Li, L., Chen, Z. M., Zhang, Y. H., Zhu, T., Li, J. L., and Ding, J.: Kinetics and mechanism of
14 heterogeneous oxidation of sulfur dioxide by ozone on surface of calcium carbonate, *Atmos.*
15 *Chem. Phys.*, 6, 2453–2464, doi:10.5194/acp-6-2453-2006, 2006.

16 Liu, Y., Gibson, E. R., Cain, J.P., Wang, H., Grassian, V. H., and Laskin, A: Kinetic Study of
17 Heterogeneous Reactions of CaCO₃ Particles with HNO₃ as a Function of Relative Humidity
18 Using Single Particle Analysis, *J. Phys. Chem. A* , 112, 1561 -1571, 2008.

19 Lo, J. C.-F., Yang, Z.-L., and PielkeSr., R. A.: Assessment of three dynamical climate
20 downscaling methods using the Weather Research and Forecasting (WRF) model, *J.*
21 *Geophys. Res.*, 113,D09112, doi:10.1029/2007JD009216, 2008.

22 Madronich, S., and Weller, G.: Numerical integration errors in calculated tropospheric
23 photodissociation rate coefficients, *J. Atmos. Chem.*, 10, 289–300, 1990.

1 Martin, R. V., Jacob, D. J., Yantosca, R. M., Chin, M., and Ginoux, P.: Global and regional
2 decreases in tropospheric oxidants from photochemical effects of aerosols, *J. Geophys. Res.*,
3 108, 4097, doi: 10.1029/2002JD002622, 2003.

4 Michel, A. E., Usher, C. R., and Grassian, V. H., Heterogeneous and catalytic uptake of ozone on
5 mineral oxides and dusts: A Knudsen cell investigation, *Geophys. Res. Lett.*, 29, 1665,
6 doi:10.1029/2002GL014896, 2002.

7 Miller, R. L., Tegen, I., and Perlwitz, J.: Surface radiative forcing by soil dust aerosols and the
8 hydrologic cycle, *J. Geophys. Res.*, 109, D04203, doi:10.1029/2003JD004085, 2004.

9 Mlawer, E. J., Taubman, S., Brown, P., Iacono, M., and Clough, S.: Radiative transfer for
10 inhomogenous atmosphere: RRTM, avalidated correlated-k model for the long-wave, *J.*
11 *Geophys. Res.*, 102, D14, doi:10.1029/97JD00237, 1997.

12 Pant, P., Hegde, P., Dumka, U. C., Satheesh, S. K., Moorthy, K. K., Saha, A., and Srivastava, M
13 . K.: Aerosol characteristics at a high-altitude location in central Himalayas: Optical
14 properties and radiative forcing, *J. Geophys. Res.*, 111, D17206, doi:
15 10.1029/2005JD006768, 2006.

16 Peterson, J. T.: Measurements of atmospheric aerosols and infrared radiation over northwest
17 India and their interrelationship, Ph. D. thesis, 165pp., Dep. Of Meteorol., Univ. of
18 Wisconsin, Madison, Wisconsin.

19 Pfister, G. G., Parrish, D. D., Worden, H., Emmons, L. K., Edwards, D. P., Wiedinmyer, C.,
20 Diskin, G. S., Huey, G., Oltmans, S. J., Thouret, V., Weinheimer, A., and Wisthaler, A.:
21 Characterizing summertime chemical boundary conditions for airmasses entering the US
22 West Coast, *Atmos. Chem. Phys.*, 11, 1769-1790, doi:10.5194/acp-11-1769-2011, 2011.

1 Pozzoli, L., Bey, I., Rast, S., Schultz, M. G., Stier, P., and Feichter, J.: Trace gas and aerosol
2 interactions in the fully coupled model of aerosol-chemistry-climate ECHAM5-HAMMOZ:
3 1. Model description and insights from the spring 2001 TRACE-P experiment, *J. Geophys.*
4 *Res.*, 113, D07308, doi: 10.1029/2007JD009007, 2008.

5 Pradhan, M., Kyriakou, G., Archibald, A. T., Papageorgiou, A. C., Kalberer, M., and Lambert,
6 R. M.: Heterogeneous uptake of gaseous hydrogen peroxide by Gobi and Saharan dust
7 aerosols: a potential missing sink for H₂O₂ in the troposphere, *Atmos. Chem. Phys.*, 10,
8 7127-7136, doi:10.5194/acp-10-7127-2010, 2010.

9 Prasad, A. K., and Singh R. P.: Changes in aerosol parameters during major dust storm events
10 (2001–2005) over the Indo-Gangetic Plains using AERONET and MODIS data, *J. Geophys.*
11 *Res.*, 112, D09208, doi:10.1029/2006JD007778, 2007.

12 Preszler Prince, A., Kleiber, P., Grassian, V. H., and Young, M. A.: Heterogeneous interactions
13 of calcite aerosol with sulfur dioxide and sulfur dioxide nitric acid mixtures, *Phys. Chem.*
14 *Chem. Phys.*, 9, 3432-3439, 2007.

15 Sagar, R., Kumar, B., Dumka, U. C., Moorthy, K. K., and Pant, P.: Characteristics of aerosol
16 optical depths over Manora Peak: A high-altitude station in the central Himalayas, *J.*
17 *Geophys. Res.*, 109, D06207, doi: 10.1029/2003JD003954, 2004.

18 Sarangi, T., Naja, M., Ojha, N., Kumar, R., Lal, S., Venkataramani, S., Kumar, A., Sagar, R. and
19 Chandola, H. C.: First simultaneous measurements of ozone, CO and NO_y at a high altitude
20 regional representative site in the central Himalayas, *J. Geophys. Res. Atmos.*, 119, 1592–
21 1611, doi: 10.1002/2013JD020631, 2014.

22 Seinfeld, J. H., Carmichael, G., Arimoto, R., Conant, W. C., Brechtel, F. J., Bates, T. S., Cahill,
23 T. A., Clarke, A. D., Doherty, S. J., Flatau, F. J., Huebert, B. J., Kim, J., Markowicz, K. M.,

1 Quinn, P. K., Russell, L. M., Russell, P. B., Shimizu, A., Y., Song, C. H., TanShag, Y., Uno,
2 I., Vogelmann, A. M., Weber, R. J., Woo, J., and Zhang, X. Y.: ACE-ASIA, Regional
3 climatic and atmospheric chemical effects of Asian dust and pollution, *B. Am. Meteor. Soc.*,
4 85, 367–380, 2004.

5 Skamarock, W. C., Klemp, J. B., Dudhia, J., Gill, D. O., Barker, D. M., Wang, W., and Powers,
6 J. G.: A description of the advancedresearch WRF version 2, NCAR Tech. Note, NCAR/TN-
7 468+STR, Natl. Cent. for Atmos. Res., Boulder, Colo, availableat: [http://wrf-
8 model.org/wrfadmin/publications.php](http://wrf-
8 model.org/wrfadmin/publications.php), 2008.

9 Tang, Y., Carmichael, G. R., Kurata, G., Uno, I., Weber, R. J., Song, C.-H., Guttikunda, S. K.,
10 Woo, J.-H., Streets, D. G., Wei, C., Clarke, A. D., Huebert, B., and Anderson, T. L.: Impacts
11 of dust on regional tropospheric chemistry during the ACE-Asia experiment: A model study
12 with observations, *J. Geophys. Res.*, 109, D19S21, doi:10.1029/2003JD003806, 2004.

13 Thompson, G., Rasmussen, R. M., and Manning, K.: Explicit forecasts of winter precipitation
14 using an improved bulk microphysics scheme, Part I: Description and sensitivity
15 analysis, *Mon. Weather Rev.*, 132, 519–542, 2004.

16 Tie, X., Madronich, S., Walters, S., Edwards, D. P., Ginoux, P., Mahowald, N., Zhang, R., Lou,
17 C., and Brasseur, G.: Assessment of the global impact of aerosols on tropospheric oxidants, *J.*
18 *Geophys. Res.*, 110, D03204, doi:10.1029/2004JD005359, 2005.

19 Underwood, G. M., Song, C. H., Phadnis, M., Carmichael, G. R., and Grassian, V. H.:
20 Heterogeneous reactions of NO₂ and HNO₃ on oxides and mineral dust: a combined
21 laboratory and modeling study, *J. Geophys. Res.*, 106, 18055–18066, 2001.

22 Usher, C. R., Michel, A. E., Stec., D. and Grassian, V. H.: Laboratory Studies of Ozone Uptake
23 on Processed Mineral Dust, *Atmos. Environ.*, 37, 5337, 2003.

1 Wagner, C., Hanisch, F., Holmes, N., de Coninck, H., Schuster, G., and Crowley, J. N.: The
2 interaction of N₂O₅ with mineral dust: aerosol flow tube and Knudsen reactor studies,
3 *Atmos. Chem. Phys.*, 8, 91–109, doi:10.5194/acp-8-91-2008, 2008.

4 Wang, K., Zhang, Y., Nenes, A., and Fountoukis, C.: Implementation of dust emission and
5 chemistry into the Community Multiscale Air Quality modeling system and initial
6 application to an Asian dust storm episode, *Atmos. Chem. Phys.*, 12, 10209-10237,
7 doi:10.5194/acp-12-10209-2012, 2012.

8 Wiedinmyer, C., Akagi, S. K., Yokelson, R. J., Emmons, L. K., Al-Saadi, J. A., Orlando, J. J.,
9 and Soja, A. J.: The Fire INventory from NCAR (FINN): a high resolution global model to
10 estimate the emissions from open burning, *Geosci. Model Dev.*, 4, 625-641,
11 doi:10.5194/gmd-4-625-2011, 2011.

12 Ying, Z., Tie, X., Madronich, S., Li, G., Massie, S.: Simulation of regional dust and its effect on
13 photochemistry in the Mexico City area during MILAGRO experiment, *Atmos. Environ.*, 45
14 (15), 2549-2558, 2011.

15 Zhang, Q., Streets, D. G., Carmichael, G. R., He, K. B., Huo, H., Kannari, A., Klimont, Z., Park,
16 I. S., Reddy, S., Fu, J. S., Chen, D., Duan, L., Lei, Y., Wang, L. T., and Yao, Z. L.: Asian
17 emissions in 2006 for the NASA INTEX-B mission, *Atmos. Chem. Phys.*, 9, 5131-5153,
18 doi:10.5194/acp-9-5131-2009, 2009.

19 Zhang, Y. and Carmichael, G. R.: The role of mineral aerosol in tropospheric chemistry in East
20 Asia - a model study, *J. Appl. Meteor.*, 38, 353–366, 1999.

21 Zhang, Y., Sunwoo, Y., Kotamarthi, V., and Carmichael, G. R.: Photochemical oxidant
22 processes in the presence of dust: An evaluation of the impact of dust on particulate nitrate
23 and ozone formation, *J. Appl. Meteor.*, 33, 813–824, 1994.

1 Zhao, C. Liu, X., Ruby Leung, L., and Hagos, S.: Radiative impact of mineral dust on monsoon
2 precipitation variability over West Africa, *Atmos. Chem. Phys.*, 11, 1879–1893,
3 doi:10.5194/acp-11-1879-2011, 2011.

4 Zhou, Y., Brunner, D., Boersma, K. F., Dirksen, R., and Wang, P.: An improved tropospheric
5 NO₂ retrieval for OMI observations in the vicinity of mountainous terrain, *Atmos. Meas.*
6 *Tech.*, 2, 401-416, doi:10.5194/amt-2-401-2009, 2009.

7 Zhu, S., Butler, T., Sander, R., Ma, J., and Lawrence, M. G.: Impact of dust on tropospheric
8 chemistry over polluted regions: a case study of the Beijing megacity, *Atmos. Chem. Phys.*,
9 10, 3855–3873, doi:10.5194/acp-10-3855-2010, 2010.

1 **Table 1:** The heterogeneous reactions and dry reactive uptake coefficients (γ_{dry}) used in this
2 study are listed. γ_{low} and γ_{high} represent lower and upper bounds of reactive uptake coefficient
3 reported in the literature. The rightmost column shows the references based on which relative
4 humidity dependence of γ_{dry} is specified.

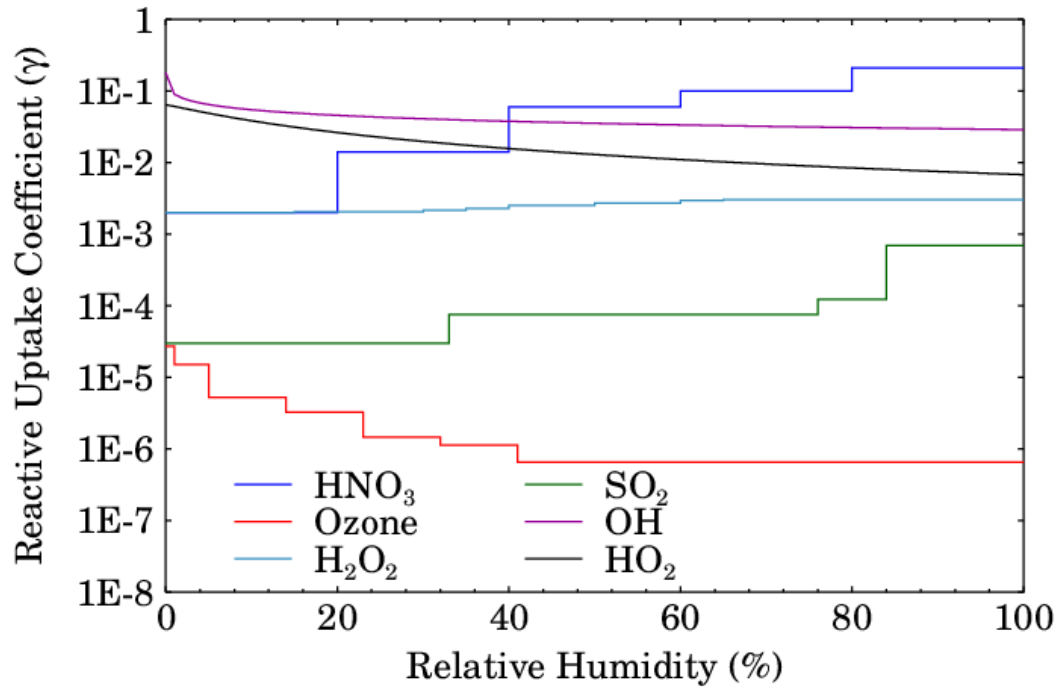
Reaction	γ_{low}	γ_{dry}	γ_{high}	RH dependence
$\text{O}_3 + \text{Dust} \rightarrow \text{P}$	1×10^{-6}	2.7×10^{-5}	1×10^{-4}	Cwiertny et al. (2008)
$\text{HNO}_3 + \text{Dust} \rightarrow 0.5 \text{NO}_x + \text{P}$	1×10^{-5}	2.0×10^{-3}	0.2	Liu et al. (2008)
$\text{NO}_2 + \text{Dust} \rightarrow \text{P}$	4×10^{-10}	2.1×10^{-6}	2×10^{-4}	-
$\text{NO}_3 + \text{Dust} \rightarrow \text{P}$	0.01	0.1	0.23	-
$\text{N}_2\text{O}_5 + \text{Dust} \rightarrow \text{P}$	0.01	0.03	0.1	-
$\text{OH} + \text{Dust} \rightarrow 0.05 \text{H}_2\text{O}_2 + \text{P}$	0.004	0.18	1	Bedjanian et al. (2013a)
$\text{HO}_2 + \text{Dust} \rightarrow 0.1 \text{H}_2\text{O}_2 + \text{P}$	0.01	6.4×10^{-2}	1	Bedjanian et al. (2013b)
$\text{H}_2\text{O}_2 + \text{Dust} \rightarrow \text{P}$	8×10^{-4}	2×10^{-3}	0.18	Pradhan et al. (2010)
$\text{SO}_2 + \text{Dust} \rightarrow \text{P}$	5×10^{-7}	3.0×10^{-5}	2.6×10^{-4}	Preszler Prince et al. (2007)
$\text{CH}_3\text{COOH} + \text{Dust} \rightarrow \text{P}$	2.4×10^{-4}	1×10^{-3}	2×10^{-3}	-
$\text{CH}_3\text{OH} + \text{Dust} \rightarrow \text{P}$	4×10^{-6}	1×10^{-5}	1.9×10^{-4}	-
$\text{CH}_2\text{O} + \text{Dust} \rightarrow \text{P}$	2.6×10^{-7}	1×10^{-5}	1.1×10^{-4}	-

5

6

1 **Table 2:** Simulations designs used in this study and their purpose are shown.

Simulation Index	Model Configuration	Purpose
No_Dust	WRF-Chem without dust emissions but other aerosols affect photolysis rates	Serves as a base simulation
Dust_J	WRF-Chem with dust emissions and all aerosols affect photolysis rates	Comparison with No_Dust will quantify the effect of dust on photolysis rates and tropospheric chemistry
Dust_JH	Same as Dust_J but with heterogeneous chemistry considering RH dependence of γ and renoxification process included	Comparison with No_Dust will yield total impact of dust on tropospheric chemistry and comparison with DUST_J will yield contribution of heterogeneous chemistry
Dust_JH_NoRH	Same as Dust_JH but RH dependence of γ is not included	Comparison with Dust_JH will provide information on RH dependence of heterogeneous uptake of gases by dust
Dust_JH_NoReNOx	Same as Dust_JH but renoxification process is not included	Comparison with Dust_JH will provide contribution of renoxification process in NOx budget.
Dust_JH_LoG	Same as Dust_JH but with lower limit of γ	Comparison with Dust_JH_HiG provides uncertainty in the effects of heterogeneous chemistry due to uncertainty in γ
Dust_JH_HiG	Same as Dust_JH but with upper limit of γ	
Dust_JH_NO ₃	Same as Dust_JH but the effect of nitrate coated dust on uptake of O ₃ is included	Comparison with Dust_JH will provide information on changes in O ₃ uptake due to coating of dust with nitrate
Dust_JH_SO ₄	Same as Dust_JH but the effect of sulfate coated dust on uptake of O ₃ is included	Comparison with Dust_JH will provide information on changes in O ₃ uptake due to coating of dust with sulfate
Dust_JH_NO ₃ _SO ₄	Same as Dust_JH but the effect of nitrate and sulfate coated dust on uptake of O ₃ is included	Comparison with Dust_JH will provide information on changes in O ₃ uptake due to coating of dust with nitrate and sulfate
Dust_JH_Sat	Same as Dust_JH but nitrate and sulfate coated particles are assumed to be saturated	Comparison with Dust_JH will provide upper limit on the effect of dust aging on the tropospheric chemistry

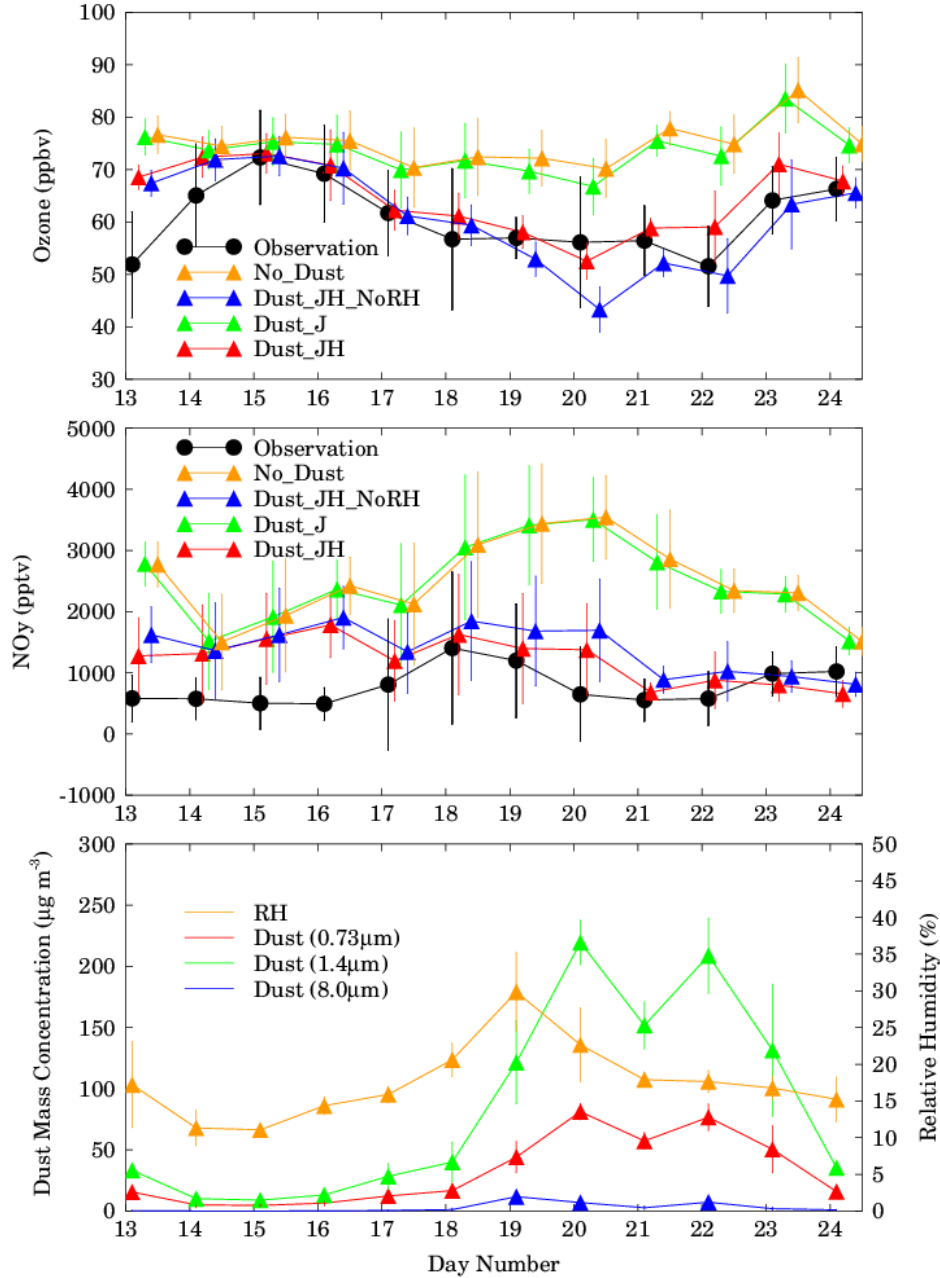


1

2 **Fig. 1:** The relative humidity dependence of reactive uptake coefficient (γ) for O₃, HNO₃, OH,

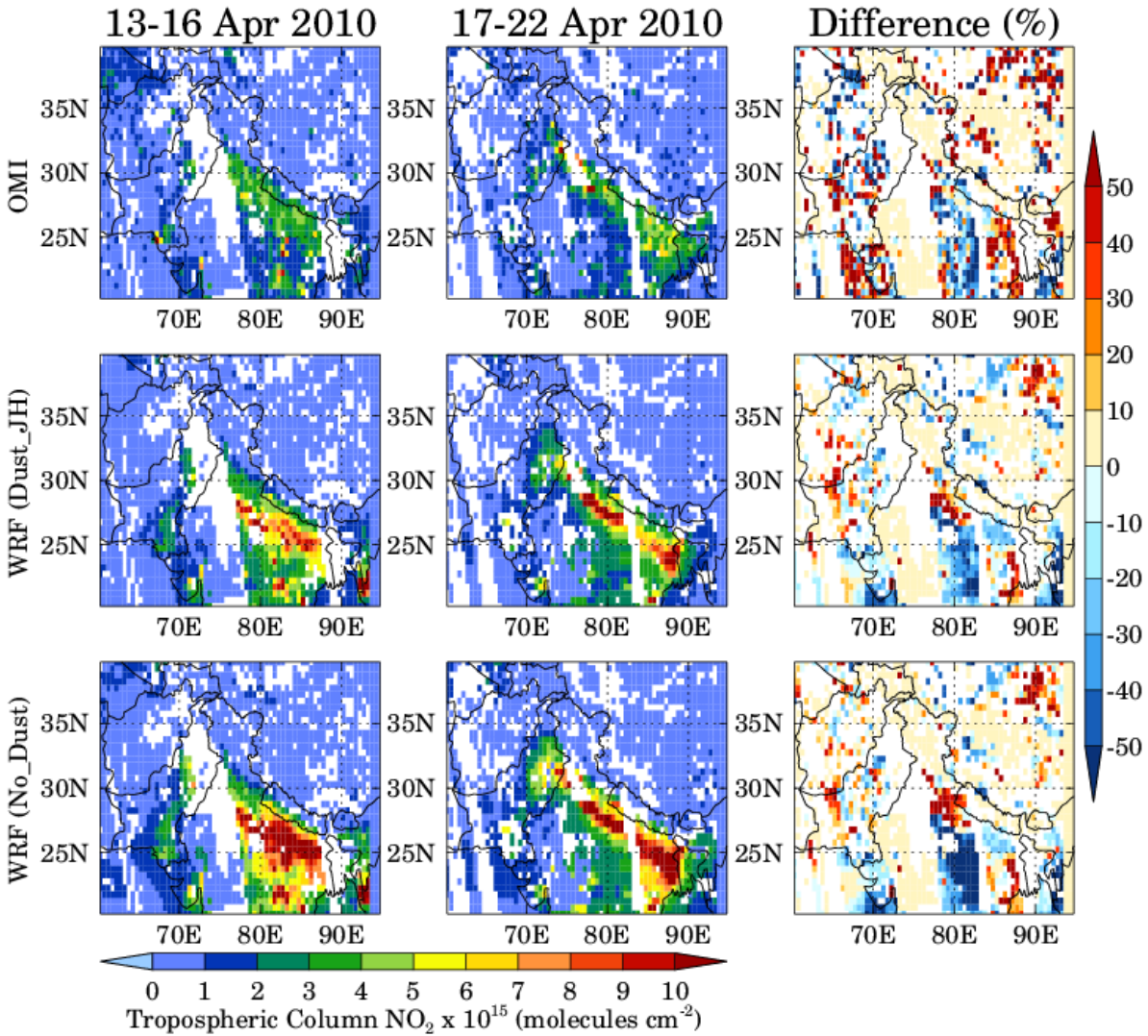
3 HO₂, H₂O₂ and SO₂ used in this study.

4



1
 2 **Fig. 2:** Variations in observed and WRF-Chem simulated (No_Dust, Dust_JH_NoRH, Dust_J
 3 and Dust_JH) daily average O₃ (top panel) and NO_y (middle panel) at Nainital during 13-24
 4 April 2010. WRF-Chem simulated daily average mass concentration of dust particles of 0.73, 1.4
 5 and 8.0 µm effective radii and relative humidity at Nainital are also shown. The vertical bars
 6 represent standard deviation in the average values.

1



2

3 **Fig. 3:** Spatial distributions of OMI retrieved and WRF-Chem (Dust_JH and No_Dust)

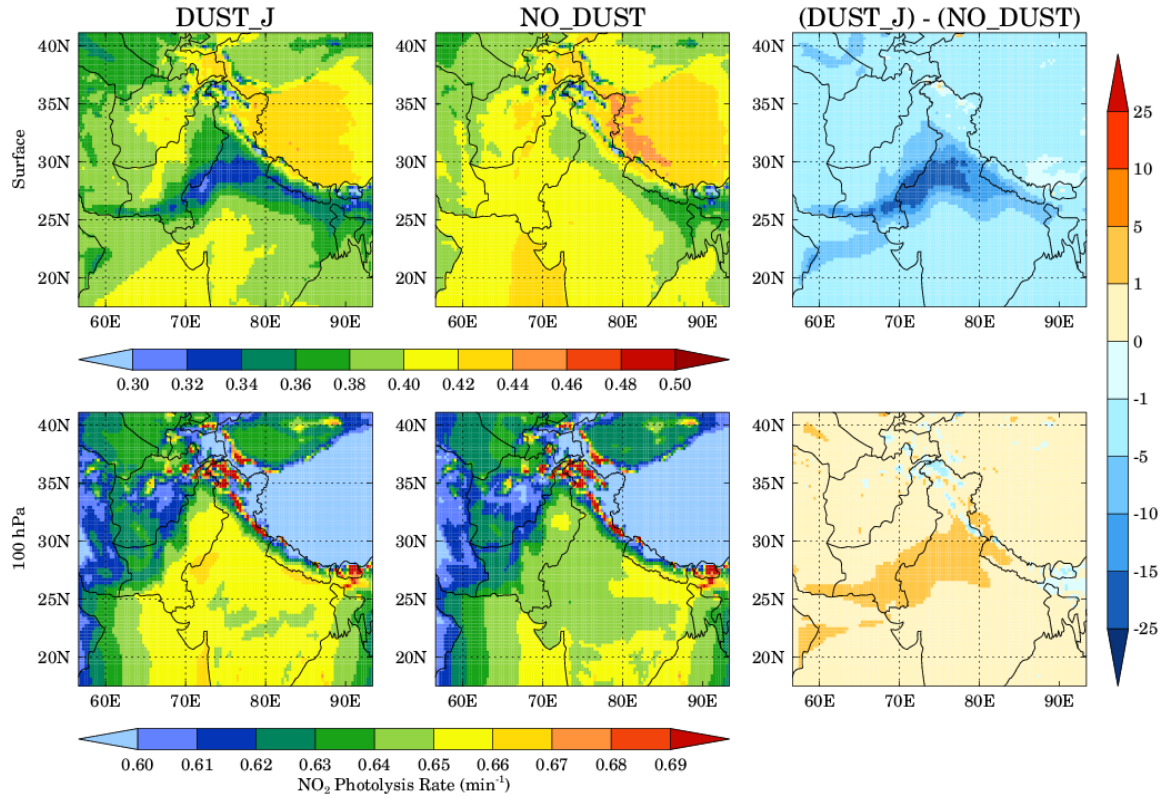
4 simulated tropospheric column NO_2 during the low (13-16 April 2010) and high (17-22 April

5 2010) dust emission periods. WRF-Chem profiles are convolved with OMI averaging kernels

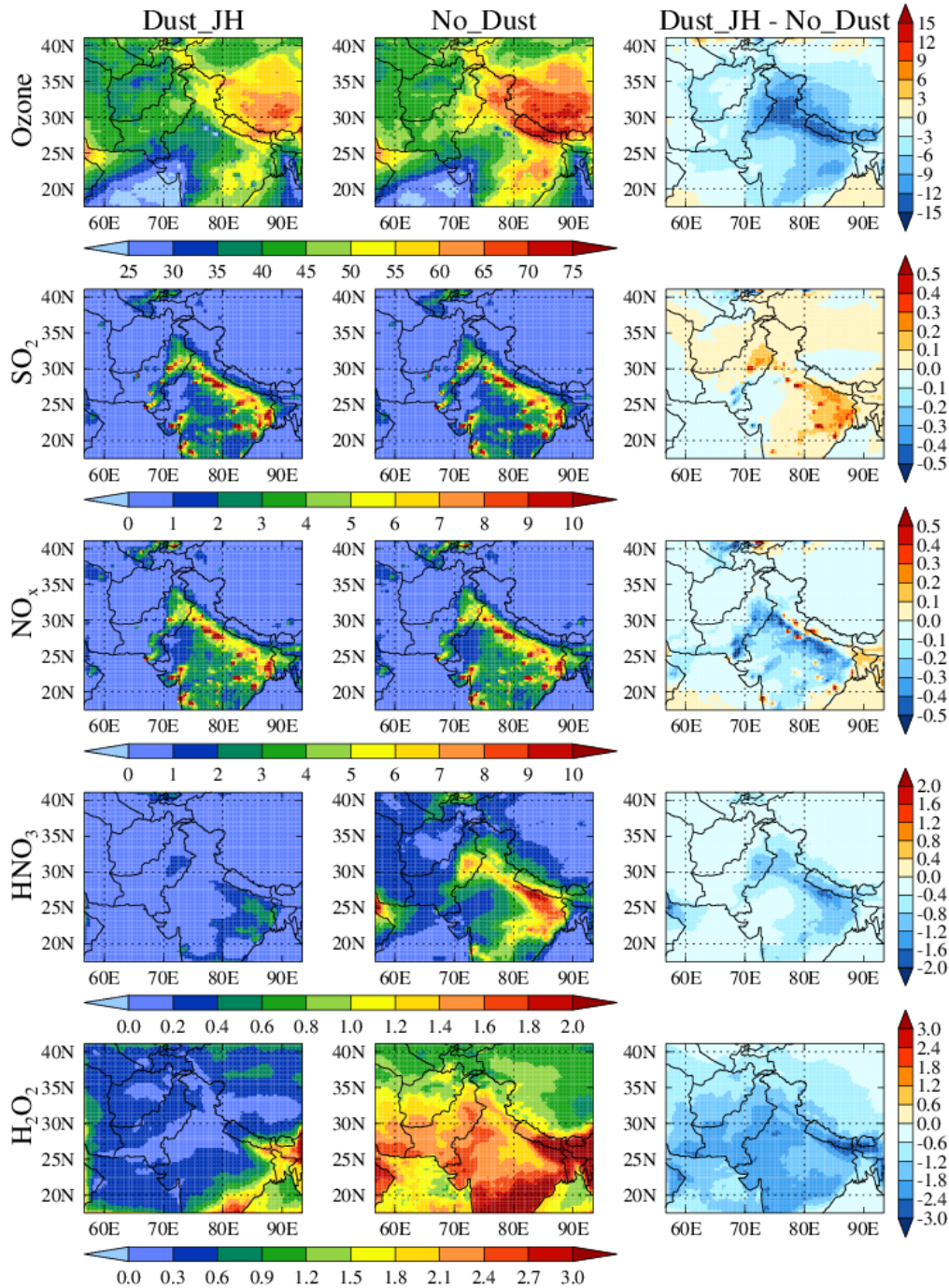
6 before comparison. The percentage differences between low and high dust emission periods are

7 also shown.

8



1
 2 **Fig. 4:** Spatial distributions of the WRF-Chem simulated daytime (0200-1200 UTC) NO₂
 3 photolysis rate with (Dust_J) and without dust (No_Dust) at the surface (top panel) and 100 hPa
 4 (bottom panel) during 17-22 April 2010 are shown. Percentage difference between Dust_J and
 5 No_Dust cases are also shown.
 6

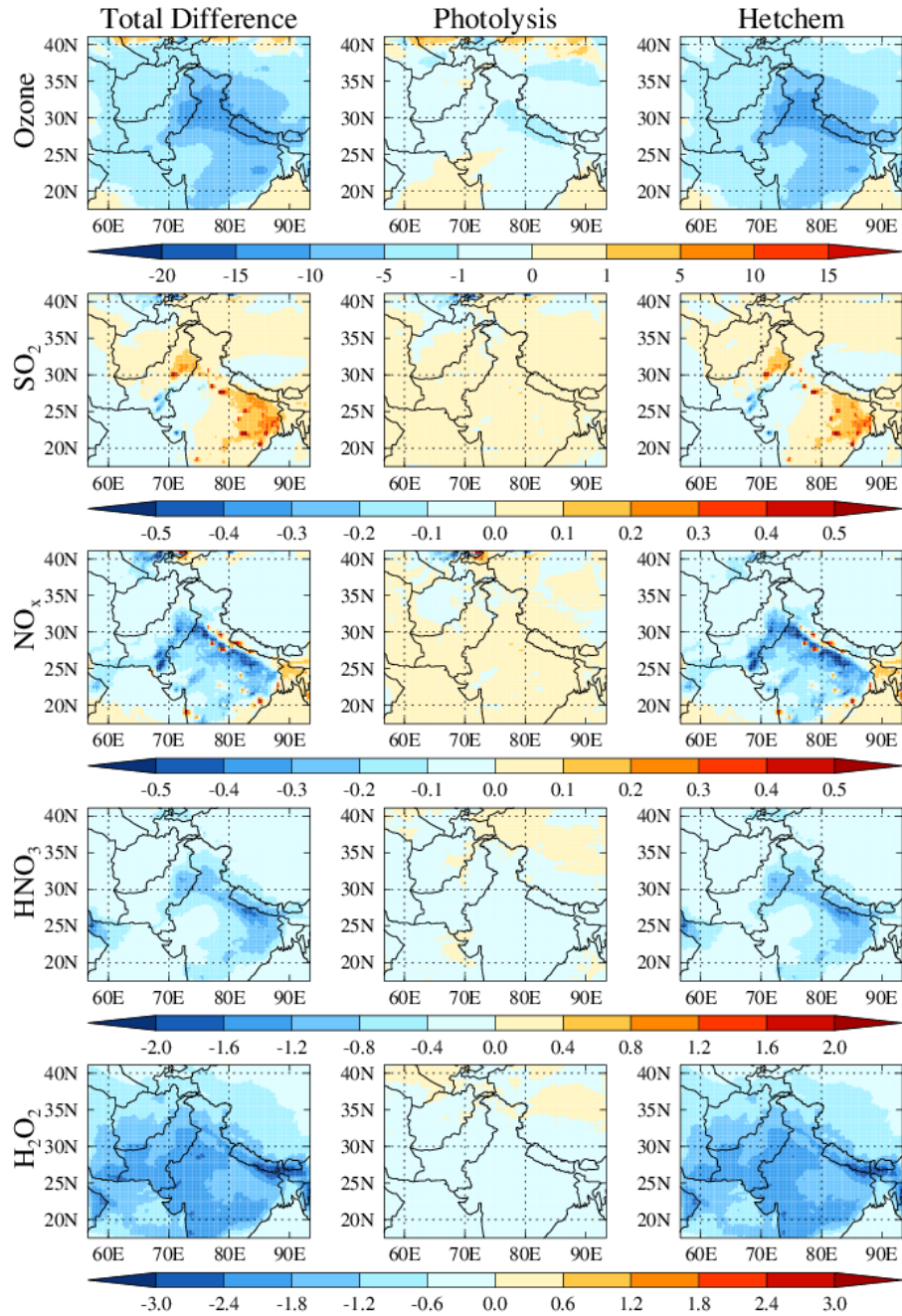


1

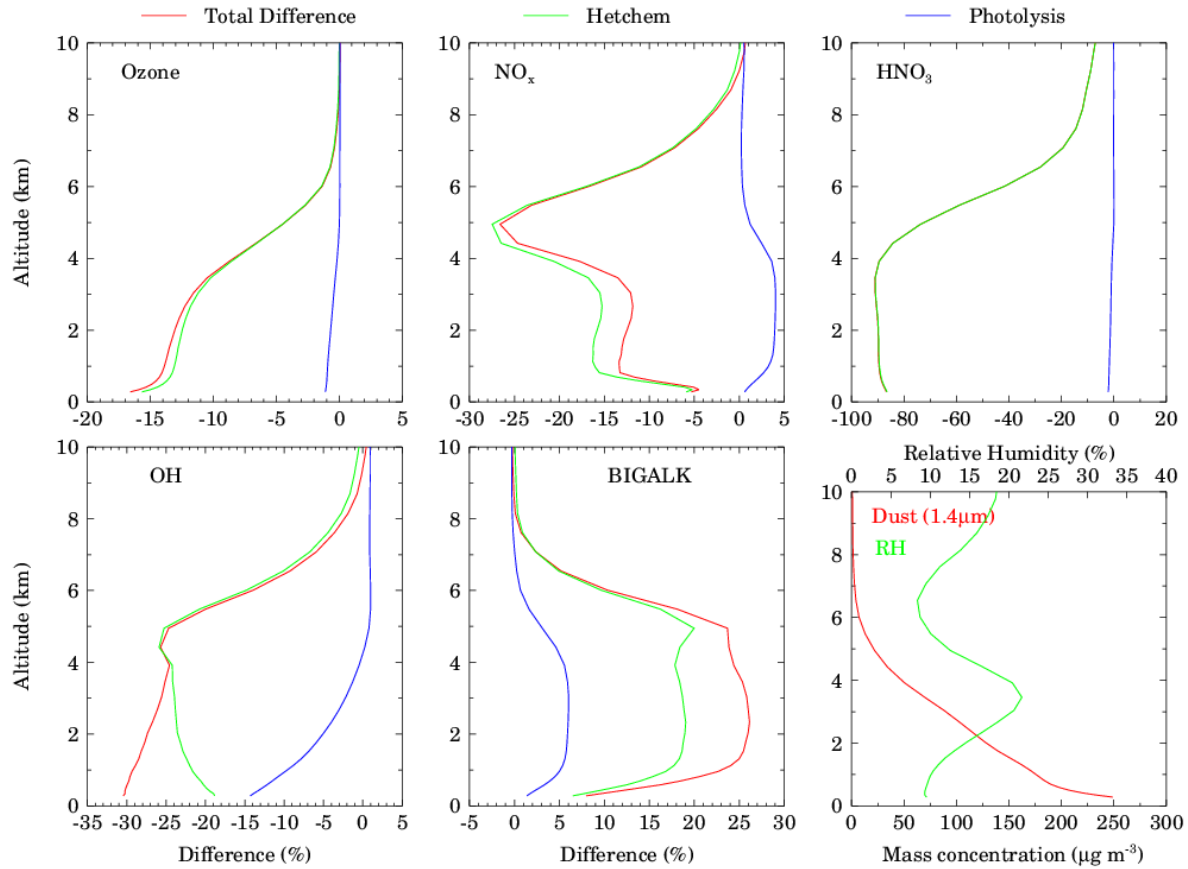
2 **Fig. 5:** Spatial distributions of average surface O₃, SO₂, NO_x, HNO₃ and H₂O₂ mixing ratios

3 simulated by WRF-Chem with Dust_JH and No_Dust configuration during 17-22 April 2010.

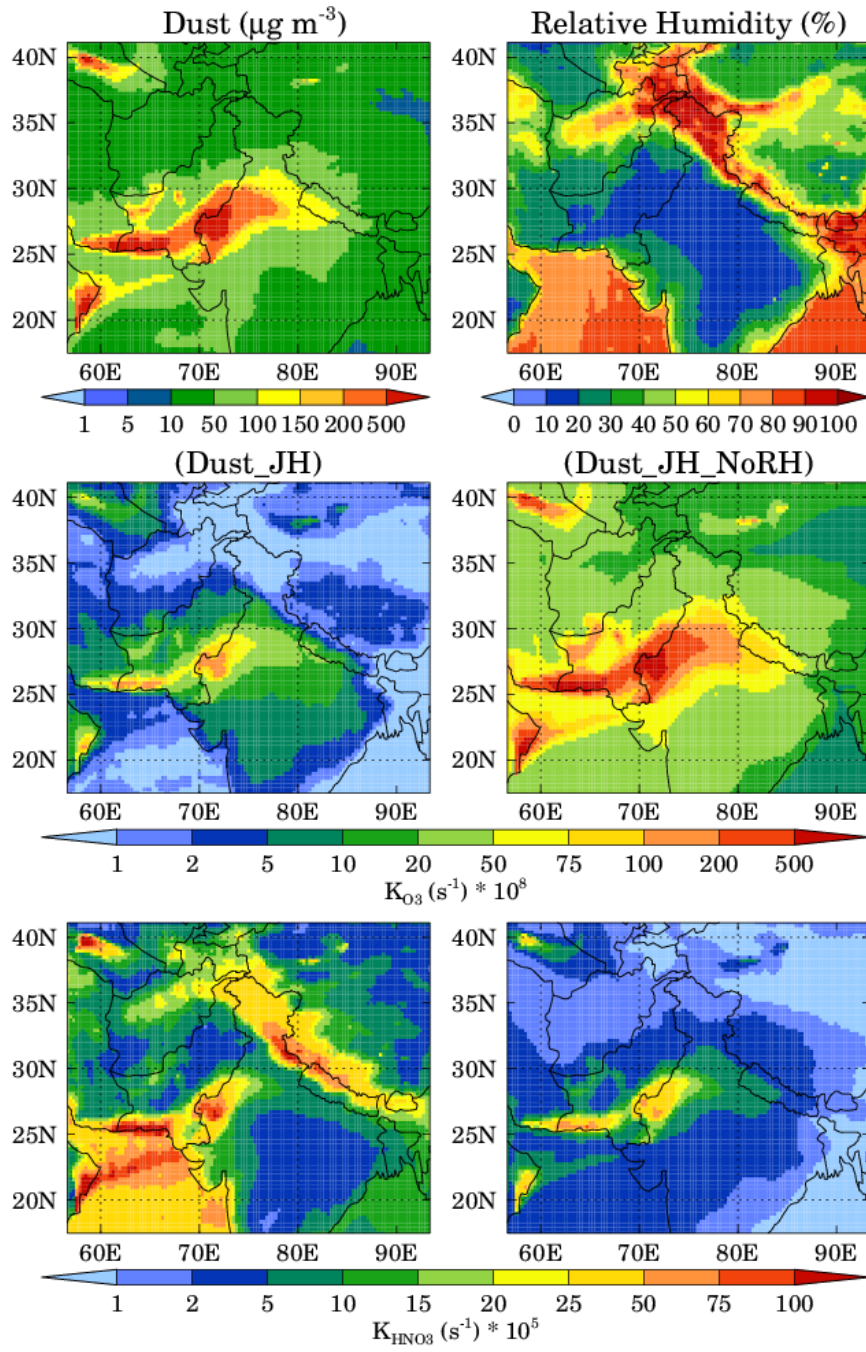
4 The absolute difference between the two configurations is also shown. All values are in ppbv.



1
 2 **Fig. 6:** Spatial distributions of absolute difference in average O₃, SO₂, NO_x, HNO₃ and H₂O₂
 3 between Dust_JH and No_Dust (left panel), Dust_J and No_Dust representing the contribution
 4 of photolysis to total difference (middle panel), and Dust_JH and Dust_J representing the
 5 contribution of heterogeneous chemistry to total differences (right panel). All values are in ppbv
 6 and for the surface layer of the model.

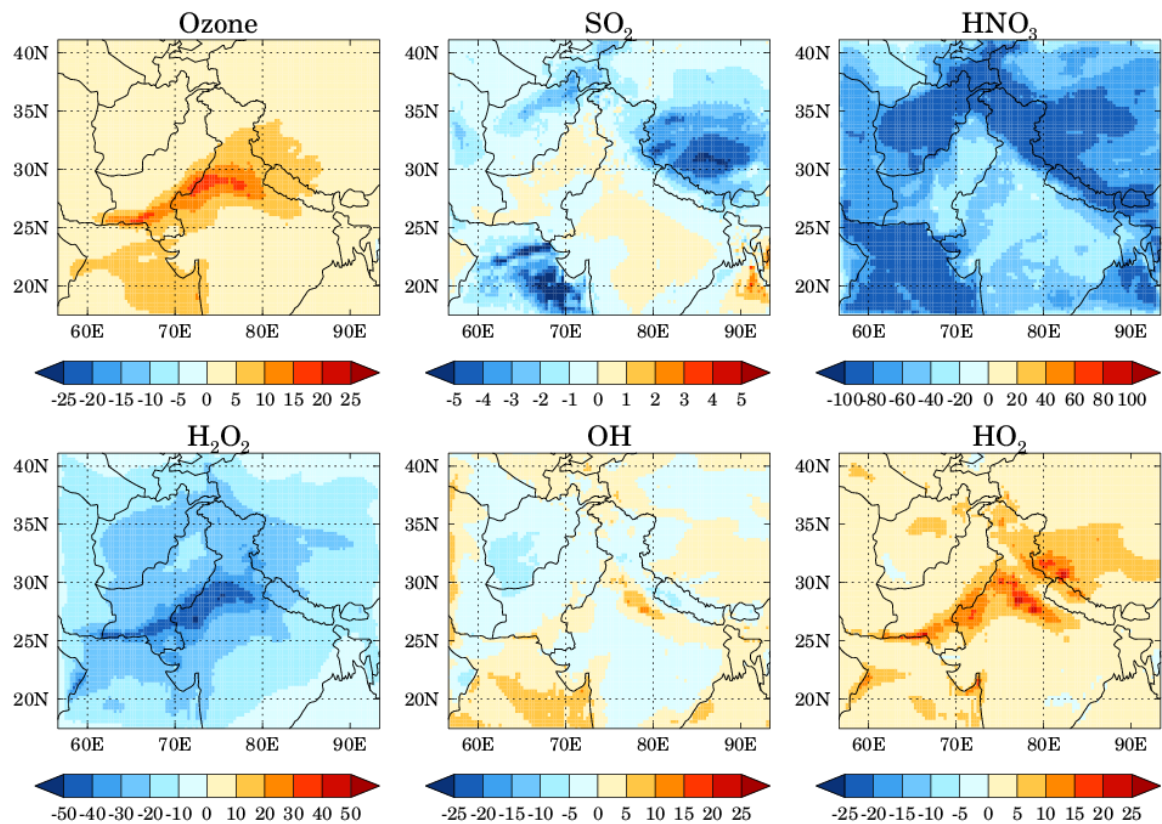


1
 2 **Fig. 7:** Vertical profiles of percentage total difference (red lines) in average O₃, NO_x, HNO₃, OH
 3 and BIGALK between Dust_JH and No_Dust configuration over the geographical region (70°-
 4 80°E, 25°-30°N) of maximum dust influence. The contributions of heterogeneous chemistry
 5 (green lines) and photolysis (blue lines) to the total percentage difference are also shown. The
 6 vertical profiles of dust mass mixing ratios for particles of 1.4 μm effective radius and relative
 7 humidity are also shown to help interpretation.

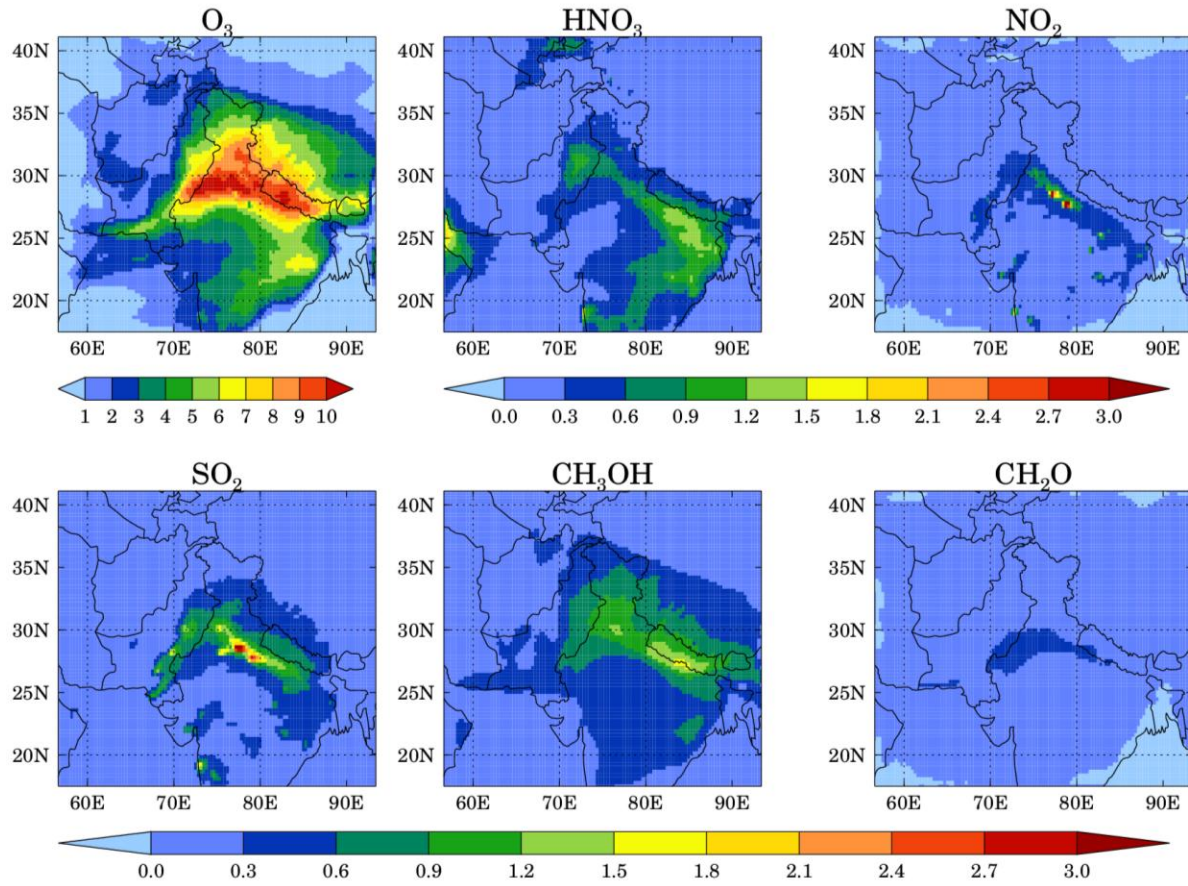


1

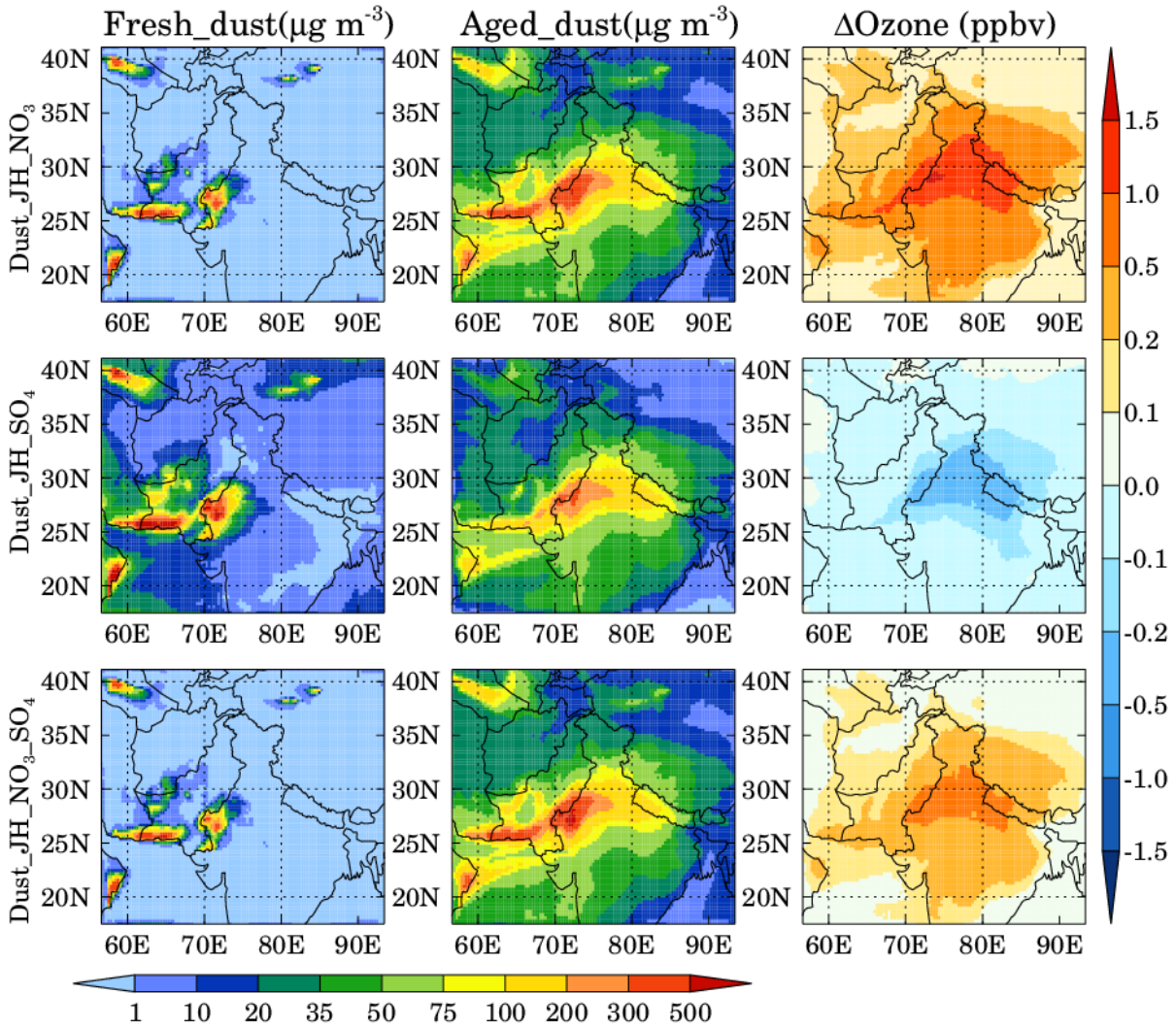
2 **Fig. 8:** Spatial distributions of average mass concentration for dust particles of 1.4 μm effective
 3 radius, relative humidity and pseudo first order rate coefficients for heterogeneous uptake of O_3
 4 (k_{O_3}) and HNO_3 (k_{HNO_3}) by dust particles in Dust_JH and Dust_JH_NoRH configurations during
 5 17-22 April 2010.



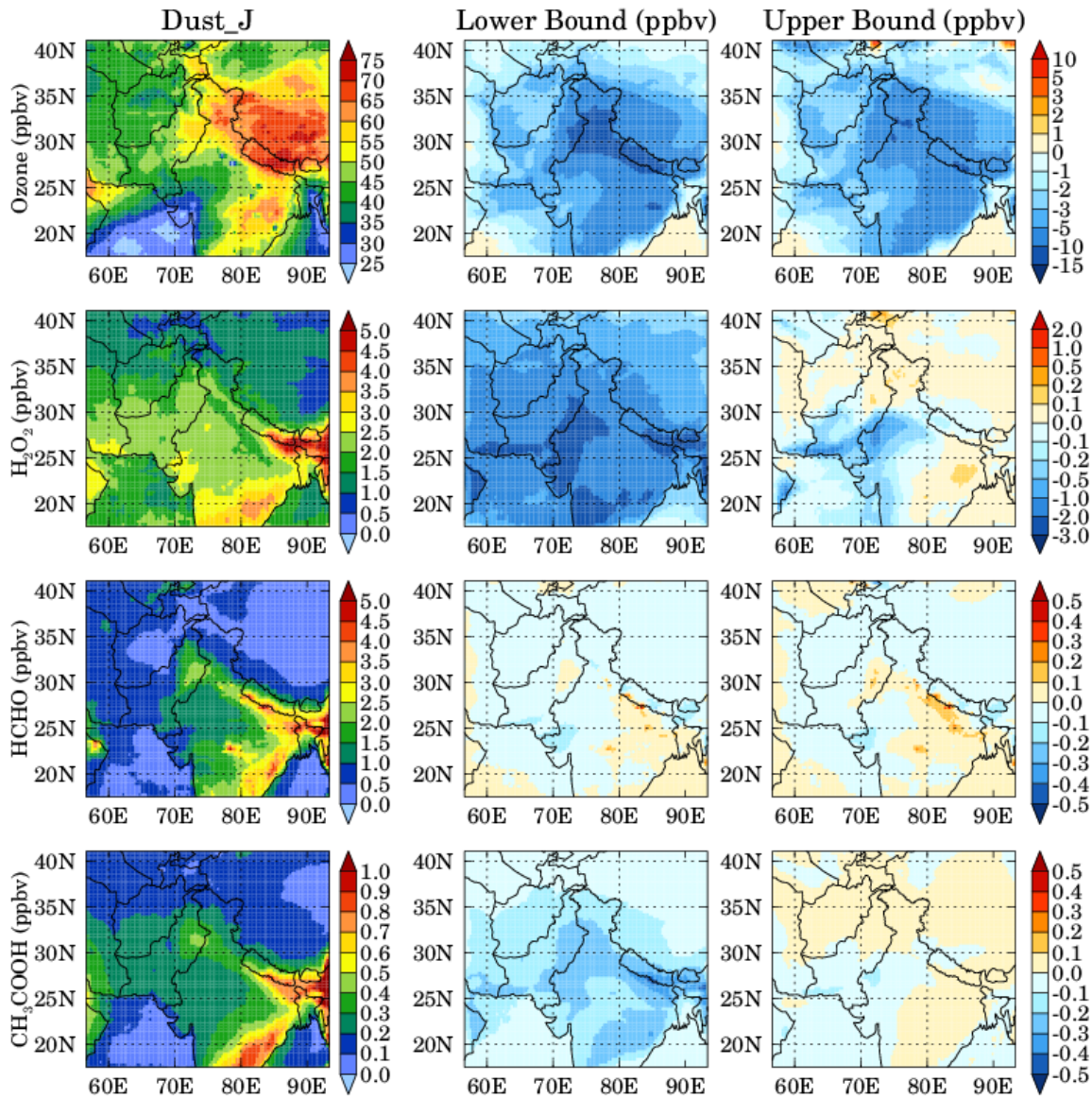
1
 2 **Fig. 9:** Spatial distributions of relative percentage differences in O₃, SO₂, HNO₃, H₂O₂, OH and
 3 HO₂ mixing ratios at the surface between Dust_JH and Dust_JH_NoRH configurations during
 4 17-22 April 2010.



1
 2 **Fig. 10:** Spatial distributions of absolute differences in O_3 , HNO_3 , NO_2 , SO_2 , CH_3OH and CH_2O
 3 surface mixing ratios between Dust_JH_LoG and Dust_JH_HiG configurations during 17-22
 4 April 2010. All values are in ppbv.



1
 2 **Fig. 11:** Spatial distributions of WRF-Chem simulated average mass concentration of fresh and
 3 aged dust particles of 1.4 μm effective radius at the surface in Dust_JH_NO₃, Dust_JH_SO₄ and
 4 Dust_JH_NO₃_SO₄ configurations during 17-22 April 2010. ΔO_3 is calculated by subtracting the
 5 average surface O₃ in Dust_JH configuration from the corresponding average values in
 6 Dust_JH_NO₃, Dust_JH_SO₄ and Dust_JH_NO₃_SO₄ configurations respectively.



1
 2 **Fig. 12:** Spatial distributions of average O₃, H₂O₂, HCHO and CH₃COOH values at the surface
 3 in Dust_J configuration, and lower and upper bounds of heterogeneous chemistry induced
 4 changes in these gases during 17-22 April 2010.

5